Resonant tidal excitation of oscillation modes in merging binary neutron stars: Inertial-gravity modes

Wenrui Xu and Dong Lai

Phys. Rev. D **96**, 083005 — Published 5 October 2017

DOI: 10.1103/PhysRevD.96.083005

Resonant Tidal Excitation of Oscillation Modes in Merging Binary Neutron Stars: Inertial-Gravity Modes

Wenrui Xu and Dong Lai
Cornell Center for Astrophysics and Planetary Science, Cornell University, Ithaca, NY 14853, USA

In coalescing neutron star (NS) binaries, tidal force can resonantly excite low-frequency ($\lesssim 500$ Hz) oscillation modes in the NS, transferring energy between the orbit and the NS. This resonant tide can induce phase shift in the gravitational waveforms, and potentially provide a new window of studying NS interior using gravitational waves. Previous works have considered tidal excitations of pure g-modes (due to stable stratification of the star) and pure inertial modes (due to Coriolis force), with the rotational effect treated in an approximate manner. However, for realistic NSs, the buoyancy and rotational effects can be comparable, giving rise to mixed inertial-gravity modes. We develop a non-perturbative numerical spectral code to compute the frequencies and tidal coupling coefficients of these modes. We then calculate the phase shift in the gravitational waveform due to each resonance during binary inspiral. Given the uncertainties in the NS equation of state and stratification property, we adopt polytropic NS models with a parameterized stratification. We derive relevant scaling relations and survey how the phase shift depends on various properties of the NS. We find that for canonical NSs (with mass $M = 1.4M_\odot$ and radius $R = 10$ km) and modest rotation rates ($\lesssim 300$ Hz), the gravitational wave phase shift due to a resonance is generally less than 0.01 radian. But the phase shift is a strong function of R and M, and can reach a radian or more for low-mass NSs with larger radii ($R \gtrsim 15$ km). Significant phase shift can also be produced when the combination of stratification and rotation gives rise to a very low frequency ($\lesssim 20$ Hz in the inertial frame) modified g-mode. As a by-product of our precise calculation of oscillation modes in rotating NSs, we find that some inertial modes can be strongly affected by stratification; we also find that the $m = 1$ r-mode, previously identified to have a small but finite inertial-frame frequency based on the Cowling approximation, in fact has essentially zero frequency, and therefore cannot be excited during the inspiral phase of NS binaries.

I. INTRODUCTION

The recent breakthrough in the detection of gravitational waves (GWs) from merging black hole (BH) binaries by advanced LIGO [1–3] heralds a new era of studying compact objects using GWs. Coalescing neutron star-neutron star (NS-NS) and NS-BH binaries have long been considered the most promising sources of GWs for LIGO/VIRGO [4, 5]. The last few minutes of the binary inspiral produce GWs with frequencies sweeping upward through the LIGO sensitivity band (10-1000 Hz). Due to the expected low signal-to-noise ratios, accurate gravitational waveforms are required to serve as theoretical templates that can be used in matched filtering to detect the GW signal from the noise and to extract binary parameters from the waveform.

The possibility of using GWs from NS binaries to constrain the equation of state (EOS) of dense nuclear matter has long been recognized [4]. The gravitational waveforms associated the final merger of two NSs or the tidal disruption of a NS by a BH exhibit power spectra with characteristic frequencies that reflect the dynamical frequency of the NS, $(GM/R^3)^{1/2}$ (where M, R are the NS mass and radius); these characteristic frequencies can be used to constrain the NS radius and thus the EOS (given the mass measurement from the inspiral waveform) (e.g., [6–12]). Since these characteristic frequencies are greater than kHz, beyond the current aLIGO sensitivity band, measuring them will be challenging without special experimental effort to enhance the high-frequency sensitivity of the LIGO interferometer.

A. Quasi-Equilibirum Tides

Another method to constrain the EOS of NSs is to use tidal effect. Numerous papers have been written on the effect of quasi-equilibirum tides on the inspiral waveforms. The quasi-equilibrium tide corresponds to the global (f-mode), quadrupolar deformation of the NS. To the leading (Newtonian) order, this tidal deformation changes the interaction potential between the two stars (with the NS mass M and radius R, the companion mass M' – treated as a point mass) from $V^{(0)}(r) = -GMM'/a$ (where a is the binary separation) to

$$V(r) = -\frac{GMM'}{a} - \mathcal{O}\left(\frac{k_2 GM'^2 R^5}{a^6}\right), \qquad (1)$$

where k_2 is the so-called Love number. This leads to a correction to the GW phase ("phase shift")

$$d\Phi = d\Phi^{(0)}\left[1 - \mathcal{O}\left(\frac{k_2 M' R^5}{M a^5}\right)\right], \qquad (2)$$

with the "point-mass" GW phase given by

$$d\Phi^{(0)} = \frac{5}{48(\pi M_c f)^{5/3}} d\ln f, \qquad (3)$$

where f is the GW frequency and $M_c = (MM')^{3/5}/(M+M')^{1/5}$ is the chirp mass. For Newtonian polytropic NS

models, simple analytic expressions (including the effect of rotation) for the phase shift are given in Ref. [13] (Eqs. 66 and 72; see also [14]). Semi-analytic GR calculations of such quasi-equilibrium tidal effect (including more precise determination of the Love number) can be found in numerous papers (e.g., [15–19]). Obviously this effect is only important at small orbital separations, just prior to merger. Again, there is some prospect of measuring this, thereby constraining the EOS, but it will be challenging because of the limited high-frequency sensitivity of aLIGO [20, 21]. At small orbital separations, there is also a "dynamical" correction to the above "equilibrium" phase shift expression [22]. This arises from the finite response time $\omega_{\rm f}^{-1}$ of the NS (where $\omega_{\rm f}$ the quadrupole f-mode frequency) as compared to the tidal forcing time $\omega_{\rm tide}^{-1}$ (where $\omega_{\rm tide} = 2\Omega$ for nonrotating NSs, with Ω the orbital frequency) [23]. This "dynamical" correction essentially amounts to replacing k_2 by $k_2/(1-4\Omega^2/\omega_{\rm f}^2)$. Thus Equation (2) becomes

$$d\Phi = d\Phi^{(0)}\left[1-\mathcal{O}\left(\frac{k_2 M' R^5}{M a^5}\right)\frac{1}{1-4\Omega^2/\omega_{\rm f}^2}\right]. \qquad (4)$$

Finally, we note that the quadrupole approximation is not accurate at small orbital separations, and one must use numerically computed quasi-equilibrium binary sequences to characterize the full tidal effects [24, 25] or use 3D hydrodynamical simulations (e.g. [8, 12]).

B. Resonant (Dynamical) Tides

In the early stage of the inspiral, with the GW frequencies between 10 Hz to a few hundred Hz, it is commonly assumed that a NS can be treated as a point mass, and tidal effects are completely negligible. This is indeed the case for the quasi-equilibrium tides discussed above. However, a NS can possess a variety of low-frequency ($\lesssim 500$ Hz) oscillation modes due to stable density stratification and/or rotation. During binary inspiral, the orbit can momentarily come into resonance with the normal modes of the NS. By drawing energy from the orbit and resonantly exciting the modes, the inspiral speeds up around the resonant frequency, giving rise to a phase shift in the GW. This problem was first studied in the case of non-rotating NSs [23, 26, 27] where the only modes that can be resonantly excited are g-modes, with typical mode frequencies $\lesssim 100$ Hz ([23, 26] considered g-modes associated with the bulk composition gradients, while [27] considered those associated with crustal density jumps). It was found that the effect is small for typical NS parameters (mass $M \simeq 1.4M_\odot$ and radius $R \simeq 10$ km) and several equations of state [23] because the coupling between the g-mode and the tidal potential is weak. Superfluidity in the NS core can significantly affect the g-mode property [28, 29], and recent studies suggest that the resulting phase shift has the same order of magnitude as that of a normal fluid NS [30, 31].

Ho & Lai (1999)[32] studied the effect of NS rotation, and found that the g-mode resonance can be strongly enhanced even by a modest rotation (e.g., the phase shift in the waveform $\Delta\Phi$ reaches up to 0.1 radian for a spin frequency $\nu_s \lesssim 100$ Hz) because rotation can reduce the g-mode frequency. For a rapidly rotating NS ($\nu_s \gtrsim 500$ Hz), f-mode resonance becomes possible (since the inertial-frame f-mode frequency can be significantly reduced by rotation) and produces a large ($\gg 1$) phase shift. They also studied the Coriolis-force driven r-modes, and found that their tidal excitations become appreciable for very rapid NS rotations. These r-modes can also be excited by (post-Newtonian) gravitomagnetic force [33], with the resulting GW phase shift comparable to the Newtonian resonant tidal excitation.

A rotating NS supports a large number of Coriolis-force driven modes named inertial modes (i-modes, also called rotational hybrid modes or generalized r-modes; see, e.g., Refs. [34–38]), of which r-mode is a member. Most i-modes have frequencies of order the NS spin frequency. Based on approximate calculations, Lai & Wu (2006) [39] found that i-modes have coupling to the Newtonian tidal potential similar to the r-modes, and most i-mode tidal resonances give relatively small GW phase shifts. They also identified one r-mode that has a rather small inertial-frame frequency, which implies a large phase shift independent of the spin frequency. This mode gives a GW frequency that is typically (for reasonable NS rotations) below the aLIGO sensitivity band (see Section IV.B.4 for our new result on this mode).

Other related studies include tidal excitation of shear modes associated with NS crusts [40] (producing small/modest phase shift) and possible nonlinear effects due to the coupling of "off-shell" f-modes to high-order g-modes and p-modes [41–43] – we will not study these issues in this paper.

C. This Paper

Overall, previous studies (reviewed above) suggest that for astrophysically most likely NS parameters ($M \simeq 1.4M_\odot$, $R \simeq 10$ km, $\nu_s \lesssim 100$ Hz), tidal resonances have a small effect on the gravitational waveform during binary inspiral (with the GW phase shift $\Delta\Phi \ll 1$). However, it is important to keep in mind that the effect is a strong function of R, and a larger NS radius ($R \simeq 15$ km), appropriate for $\sim 1.4M_\odot$ NSs with stiff EOS or low-mass ($\lesssim 1M_\odot$) NSs, would significantly increase the phase shift. In the case of g-modes, the magnitude of $\Delta\Phi$ depends on several uncertain aspects of nuclear EOS (e.g. the symmetry energy). Although the observed double NS systems all have rather modest rotation rates ($\lesssim 50$ Hz), rapidly rotating NSs (~ 700 Hz) have been found. Future GW observations may reveal new classes of NSs that are totally different from those already observed via electromagnetic radiation. To this end, it is desirable to examine tidal resonances for a wide

range of NS parameters and survey various possibilities. This is one of the main goals of this paper.

Previous studies of inertial mode resonances during binary inspiral have adopted approximate calculation of these modes. Given that the GW phase shift due to resonance depends on the tidal coupling coefficient, which in turn depends sensitively on the shape of the mode wavefunction, there is a concern that an inaccurate treatment may lead to large error. Indeed, we show in this paper that one of the "important" r-modes identified in Ref. [39] turns out to have identically zero frequency (see Section IV.B). Moreover, previous calculations of the mixed "inertial-gravity" modes of NSs are not accurate, particularly in the regime where stratification and Coriolis force are comparable – and it is precisely in this regime (where the mode frequency is close to zero in the inertial frame) that a significant phase shift is expected. Note that accurate calculations of mixed modes in main-sequence stars [44] and NSs [38] do exist (the latter use an initial-value problem to determine mode frequencies but not eigenfunctions), but they do not calculate the tidal coupling coefficients of the modes. In this paper, we develop a new spectral code to calculate the inertial-gravity modes (both the frequency and tidal coupling coefficient) precisely, including the full treatment of Coriolis force, gravitational potential perturbation and the effect of rotational distortion, and we use the results to evaluate the significance of tidal resonances of stratified, rotating NSs.

Our paper is organized as follows. Section II summarizes the key equations for calculating the gravitational wave phase shift due to tidal resonance. Section III describes our method for numerical computation of the oscillation modes of rotating, stratified NSs. In Section IV we discuss the key results of NS oscillation modes (including scaling relations) that directly influence resonant tidal excitation. We present our results for the GW phase shifts associated with various mode resonances in Section V and conclude in Section VI.

II. TIDAL RESONANCE DURING BINARY INSPIRAL

The method of calculating the GW phase shift due to tidal resonance in a rotating NS with arbitrary spin-orbit misalignment was presented in Refs. [32, 39]. Here we introduce the notations and give the key equations.

Consider a NS of mass M, radius R and spin $\mathbf{\Omega}_s$ in orbit with a companion of mass M' (another NS or a black hole). We allow for a general spin-orbit inclination angle Θ (the angle between $\mathbf{\Omega}_s$ and the orbital angular momentum $\mathbf{L}$). The orbital radius a decreases and the orbital angular frequency $\Omega_{\rm orb}$ increases in time due to GW emission. In the spherical coordinate system centered on M with the Z-axis along $\mathbf{L}$, the gravitational potential produced by M' is (to quadrupole order):

$$U(\mathbf{r},t) = -\frac{GM'r^2}{a^3}\left(\frac{3\pi}{10}\right)^{1/2}\Big[e^{-2i\Phi_{\rm orb}(t)}Y_{22}(\theta_L,\phi_L) + e^{2i\Phi_{\rm orb}(t)}Y_{2,-2}(\theta_L,\phi_L)\Big], \tag{5}$$

where $\Phi_{\rm orb}(t)=\int^t dt\,\Omega_{\rm orb}$ is the orbital phase. We ignore higher order components of the tidal potential since they have little contribution to the tidal coupling.

In order to describe oscillation modes relative to the spin axis, we express the tidal potential in terms of $Y_{lm}(\theta,\phi)$, the spherical harmonic function defined in the corotating frame of the NS with the z-axis along $\mathbf{\Omega}_s$. This is achieved by the relation

$$Y_{2m'}(\theta_L,\phi_L) = \sum_m \mathcal{D}^{(2)}_{mm'}(\Theta)Y_{2m}(\theta,\phi_s), \tag{6}$$

where $\mathcal{D}^{(2)}_{mm'}$ is the Wigner $\mathcal{D}$-function and $\phi_s=\phi+\Omega_s t$.

Oscillation modes of the NS are specified by the Lagrangian displacement, $\boldsymbol{\xi}(\mathbf{r},t)$, of a fluid element from its unperturbed position. In the rotating frame, a free mode of frequency ω_α has $\boldsymbol{\xi}_\alpha(\mathbf{r},t)=\boldsymbol{\xi}_\alpha(\mathbf{r})\,e^{-i\omega_\alpha t}\propto e^{im\phi-i\omega_\alpha t}$, where m is the azimuthal number of the mode and α denotes the mode index (which includes m). We only need to consider $m>0$, since a mode with (m,ω_α) is physically identical to a mode with $(-m,-\omega_\alpha)$. In this convention ($m>0$), a mode with $\omega_\alpha>0$ ($\omega_\alpha<0$) is prograde (retrograde) with respect to the rotation.

A tidal resonance occurs when a mode with the inertial-frame frequency

$$\sigma_\alpha = \omega_\alpha + m\Omega_s, \tag{7}$$

is excited by the potential component $\propto e^{-im'\Phi_{\rm orb}}$, with the mode frequency satisfying the condition

$$\sigma_\alpha = m'\Omega_{\rm orb}. \tag{8}$$

Note that for quadrupolar tide, we only need to consider $m'=\pm 2$. Clearly, a prograde mode ($\sigma_\alpha>0$) is excited by the $m'=2$ potential, while a retrograde mode ($\sigma_\alpha<0$) by the $m'=-2$ potential. The energy transferred to the mode during the resonance is given by

$$\Delta E_{\alpha,m'} = \frac{3\pi}{10}\frac{GM'^2}{R}\frac{GM}{R^3}\left(\frac{\pi}{m'\dot{\Omega}_{\rm orb}}\right)\frac{\sigma_\alpha}{\varepsilon_\alpha} \times\left(\mathcal{D}^{(2)}_{mm'}Q_{\alpha,2m}\right)^2\left(\frac{R}{a_\alpha}\right)^6, \tag{9}$$

where $\dot{\Omega}_{\rm orb}$ is the rate of change of $\Omega_{\rm orb}$ due to GW emission, a_α is the binary semi-major axis at the tidal resonance, and

$$Q_{\alpha,2m} \equiv \langle \boldsymbol{\xi}_\alpha, \nabla(r^2Y_{2m})\rangle, \tag{10}$$

$$\varepsilon_\alpha \equiv \omega_\alpha + \langle \boldsymbol{\xi}_\alpha, i\mathbf{\Omega}_s\times\boldsymbol{\xi}_\alpha\rangle, \tag{11}$$

with $\langle A,B\rangle \equiv \int d^3x\rho(A^*\cdot B)$, and we use the normalization $M=R=1$ and $\langle \boldsymbol{\xi}_\alpha,\boldsymbol{\xi}_\alpha\rangle = 1$. The quantity $Q_{\alpha,2m}$ is a nondimensional number characterizing the strength of the tidal coupling of the mode. The phase shift in GW signal caused by this energy transfer is given by

$$\Delta\Phi = -\frac{5\pi^2}{1024}\left(\frac{Rc^2}{GM}\right)^5 \frac{1}{q(1+q)} \times \frac{m'}{\hat{\varepsilon}_\alpha|\hat{\sigma}_\alpha|}\left(\mathcal{D}^{(2)}_{mm'}Q_{\alpha,2m}\right)^2, \tag{12}$$

where $\hat{\sigma}_\alpha = \sigma_\alpha(R^3/GM)^{1/2}$ and $\hat{\varepsilon}_\alpha = \varepsilon_\alpha(R^3/GM)^{1/2}$. Note that in the above equation, $m' = \pm 2$ and $m = 1$ or 2; modes with larger m do not couple with the quadrupole tidal potential.

Note that when the binary consists of two NSs with comparable mass, each of them experiences tidal resonances caused by the other. The tidal resonances on the two NSs in general happen at different $\Omega_{\rm orb}$ unless they have exactly the same mass, radius and spin. Meanwhile, the width of a tidal resonance is very narrow [see Eqs.(2.44)-(2.45) of [32]], so resonances on the two NSs do not interfere with one another, and the total phase shift is simply the sum of the phase shifts of the resonances on each of the NSs.

III. MODES IN ROTATING NEUTRON STARS: METHOD OF CALCULATION

This section describes our numerical method to calculate the oscillation modes of rotating, stratified neutron stars. For simplicity, we assume the equilibrium state of the NS to be barotropic and spherically symmetric, i.e., the centrifugal distortion due to rotation is ignored; this should not affect our lowest order results when Ω_s is relatively small compared to $(GM/R^3)^{1/2}$. (For one particular inertial mode, the effect of centrifugal distortion can be important – this will be discussed in Section IV.B). We include the full effects of the Coriolis force and gravitational potential perturbation in the mode calculation.

The numeric code we use here is based on the spectral method developed by Reese et al. (2006) [45] to calculate p-modes in rapidly rotating and stratified stars with polytropic density profile and stratification characterized by a constant adiabatic exponent. We modify this method to allow for general density and stratification profiles. Reese et al. also included the distortion of the star due to rotation in their calculation. For most part of this paper we ignore this distortion for simplicity, but its effect can be incorporated in our method without much technical difficulty (see Section IV.B.2).

Let the equilibrium (unperturbed) stellar profile be given by density $\rho_0(r)$, pressure $p_0(r)$ and gravitational potential $\Psi_0(r)$. In the rotating frame, the Eulerian perturbation of density, pressure and gravitational potential are denoted by $\delta\rho, \delta p$ and $\delta\Psi$, respectively. The velocity perturbation $\delta\mathbf{v}$ is related to the Lagrangian displacement $\boldsymbol{\xi}$ by $\delta\mathbf{v} = -i\omega\boldsymbol{\xi}$, where we have assumed $\boldsymbol{\xi}\propto e^{-i\omega t}$ and ω is the mode frequency in the rotating frame. The linearized fluid dynamics equations then reduce to a generalized eigenvalue problem:

$$-i\omega\delta\rho = -\nabla\cdot(\rho_0\delta\mathbf{v}), \tag{13}$$

$$-i\omega\rho_0\delta\mathbf{v} = -\nabla\delta p + \delta\rho\mathbf{g}_0 - \rho_0\nabla\delta\Psi - 2\rho_0\boldsymbol{\Omega}_\mathbf{s}\times\delta\mathbf{v}, \tag{14}$$

$$-i\omega(\delta p - c_0^2\delta\rho) = \frac{\rho_0 N_0^2 c_0^2}{||\mathbf{g}_0||^2}\delta\mathbf{v}\cdot\mathbf{g}_0, \tag{15}$$

$$0 = \Delta\delta\Psi - 4\pi G\delta\rho. \tag{16}$$

The gravitational acceleration $\mathbf{g}_0$, addiabatic sound speed c_0 and Brunt-Väisälä frequency N_0 are given by

$$\mathbf{g}_0 = -\nabla\Psi_0, \tag{17}$$

$$c_0^2 = \Gamma\frac{p_0}{\rho_0}, \tag{18}$$

$$N_0^2 = \mathbf{g}_0\cdot\frac{\nabla\rho_0}{\rho_0}\left(1-\frac{\gamma}{\Gamma}\right), \tag{19}$$

where γ and Γ are defined by

$$\gamma \equiv \frac{d\ln p_0}{d\ln\rho_0}, \tag{20}$$

$$\Gamma \equiv \left(\frac{\partial\ln p}{\partial\ln\rho}\right)_{\rm ad}. \tag{21}$$

The subscript "ad" denotes adiabatic derivative. In general Γ and γ depend on r. When the star has a polytropic density profile, γ is constant and corresponds to the polytropic exponent.

To solve the eigenvalue problem, we decompose $\delta\mathbf{v}$ into spheroidal and toroidal components:

$$\delta\mathbf{v} = \sum_{j=m}^{\infty}\Big[u_{jm}Y_{jm}\mathbf{e}_r + v_{jm}\left(\partial_\theta Y_{jm}\mathbf{e}_\theta + D_\phi Y_{jm}\mathbf{e}_\phi\right) + w_{jm}\left(D_\phi Y_{jm}\mathbf{e}_\theta - \partial_\theta Y_{jm}\mathbf{e}_\phi\right)\Big], \tag{22}$$

where u_{jm}, v_{jm}, w_{jm} are functions of r, $\mathbf{e}_r, \mathbf{e}_\theta, \mathbf{e}_\phi$ are unit vectors in the r,θ,ϕ directions, respectively, and $D_\phi \equiv (\sin\theta)^{-1}\partial_\phi$. The terms with u_{jm}, v_{jm} give the spheroidal component of the velocity perturbation and the terms with w_{jm} the toroidal component.

More details of our spectral algorithm are given in the Appendix (see also Ref. [45]), where we also discuss the limitation of the method.

IV. OSCILLATION MODES AND TIDAL COUPLING COEFFICIENTS

There have been numerous theoretical studies of NS oscillations, taking account of "realistic" NS structure

and equation of state (including stratification, superfluidity, crustal rigidity, etc.) and general relativity (e.g., [46, 47]). While for non-rotating NSs, the computation of various non-radial modes (for a given NS model) can be achieved efficiently, for rotating NSs, there remain appreciable technical challenges to compute oscillation modes in the non-perturbative regime (e.g., [38, 48]; see [49] for a review). Given the uncertainty in the NS interior equation of state, in this paper we mainly consider Newtonian polytropic models (both in terms of the density profile and stratification), in order to provide a survey of different possibilities and to identify the most important oscillation modes for tidal resonance.

A. Pure g-Modes

1. G-mode Scaling Relations

For non-rotating NSs ($\Omega_s = 0$), only gravity modes (g-modes) have sufficiently low frequencies to allow resonant excitation during binary inspiral. G-modes in NSs arise from composition (e.g. proton to neutron ratio) gradient in the stellar core [50], density discontinuities in the crust [51, 52] as well as thermal buoyancy associated with finite temperatures [46]. For cold NSs (as expected in merging binaries), the composition gradient in the core provides the strongest restoring force. The core g-modes are sensitive to the symmetry energy of nuclear matter [23], and are also affected by the presence of superfluidity (in which case the restoring force for g-modes arise from the gradient in muon-to-electron fraction; see [28, 29]). Here for simplicity we first consider polytropic NS models with constant $\gamma = 2$ and constant adiabatic index $\Gamma > \gamma$. We vary Γ to survey different strength of stratification. This model should give a relatively good estimation of the frequency and tidal coupling of g-modes in realistic NSs.

G-modes are purely spheroidal [i.e. $w_{jm} = 0$ in Eq. (22)] and has only one nonzero j component. Thus we can label a mode by three numbers, j, m and n, where n corresponds to the number of nodes in u_{jm}. Because of the symmetry, the mode frequency and tidal coupling coefficient depend only on j and n. Only $j = 2$ modes couple to the quadrupole ($l = 2$) tidal potential.

The middle two columns in Table I give the scaled frequency and tidal coupling coefficient of $j = 2$ g-modes with different n for a $\gamma = 2$ polytropic NS. Our numerical results show that (to lowest order)

$$\omega_\alpha \propto (\Gamma - \gamma)^{1/2} M^{1/2} R^{-3/2}, \tag{23}$$

$$Q_{\alpha,2m} \propto \Gamma - \gamma, \tag{24}$$

so we define scaled frequency and tidal coupling coefficient by

$$\bar{\omega}_\alpha = \omega_\alpha \left(\frac{\Gamma - \gamma}{0.01}\right)^{-1/2} M_{1.4}^{-1/2} R_{10}^{3/2}, \tag{25}$$

$$\bar{Q}_{\alpha,2m} = Q_{\alpha,2m} \left(\frac{\Gamma - \gamma}{0.01}\right)^{-1}, \tag{26}$$

where $M_{1.4} = M/(1.4M_\odot)$ and $R_{10} = R/(10\,\mathrm{km})$. This scaling ensures that the results are independent of the NS mass, radius and stratification ($\Gamma - \gamma$) when $\Gamma - \gamma \ll 1$. Note that the scaled variables are equal to the physical frequency and tidal coupling coefficient for a canonical NS with $M = 1.4M_\odot, R = 10$ km and $\Gamma - \gamma = 0.01$. The $(\Gamma - \gamma)$ scaling of ω_α we obtain agrees with the analytical WKB estimate of the mode frequency (e.g. [23])

$$\omega_\alpha \simeq \frac{\sqrt{j(j+1)}}{(n+C)\pi} \int_0^R \frac{N_0(r)}{r} dr, \tag{27}$$

where C is a constant of order unity, and the Brunt-Väisälä frequency $N_0(r)$ is given by

$$N_0(r) = g_0 \sqrt{\frac{\rho_0}{p_0}} \left(\frac{1}{\gamma} - \frac{1}{\Gamma}\right)^{1/2}, \tag{28}$$

which is proportional to $(\Gamma - \gamma)^{1/2}$ for $(\Gamma - \gamma) \ll 1$.

We see from Table I that $Q_{\alpha,2m}$ decreases significantly with increasing n; therefore the $n = 1$ g-modes are the only modes that contribute significantly to the phase shift induced by tidal resonances. Note that for realistic NS stratification ($\Gamma - \gamma \sim 0.01$), the tidal coupling is small even fore the $n = 1$ modes.

2. Effect of Different Stellar Density Profiles

Canonical NSs with mass around $1.4M_\odot$ can be approximated by a polytrope with γ between 2 and 3, and low-mass ($\lesssim 1M_\odot$) could be modeled with $\gamma = 1.5$. Therefore, it is useful to investigate how different NS density profiles (different γ) affect the g-modes. Table I contains the scaled frequency and tidal coupling coefficient of g-modes for two other NS models. One of them is a $\gamma = 1.5$ polytrope. The other has

$$\gamma(r) = 2 + \tanh\left[\frac{5\rho_0(r)}{\rho_c}\right], \tag{29}$$

with ρ_c the central density of the NS; this model has $\gamma \simeq 3$ except for a thin layer near the surface where γ drops to 2. This model is chosen because our spectral algorithm requires the NS to have $\gamma \leq 2$ at the surface (see more discussion in Appendix); realistic NSs do have $\gamma \lesssim 2$ near the surface. This model should be a reasonably good approximation for a $\gamma = 3$ polytrope, thus we call it the "$\gamma \simeq 3$" model. For both $\gamma = 1.5$ and $\gamma \simeq 3$ models we also assume a constant $\Gamma - \gamma$, so the scaling (25) - (26) can still be used.

TABLE I. Scaled frequency and tidal coupling coefficient[a] for $j = 2$ pure g-modes in NSs with different density profiles, assuming constant $\Gamma - \gamma$.

	$\gamma = 1.5$		$\gamma = 2$		$\gamma \simeq 3$[b]	
	$\bar{\omega}_\alpha$ $(2\pi\text{Hz})$	$\bar{Q}_{\alpha,2m}$	$\bar{\omega}_\alpha$ $(2\pi\text{Hz})$	$\bar{Q}_{\alpha,2m}$	$\bar{\omega}_\alpha$ $(2\pi\text{Hz})$	$\bar{Q}_{\alpha,2m}$
$n = 1$	± 429	1.2×10^{-3}	± 181.3	3.5×10^{-4}	± 92.8	7.5×10^{-5}
$n = 2$	± 309	5.2×10^{-4}	± 124.6	8.5×10^{-5}	± 61.7	1.2×10^{-5}
$n = 3$	± 242	2.4×10^{-4}	± 95.7	2.5×10^{-5}	± 46.9	3×10^{-6}

[a] The scaled quantities are defined by Eqs. (25)-(26).
[b] This model has $\gamma \simeq 3$ except for a thin layer near the surface where γ drops to 2. For details of this model see Section IV.A.2.

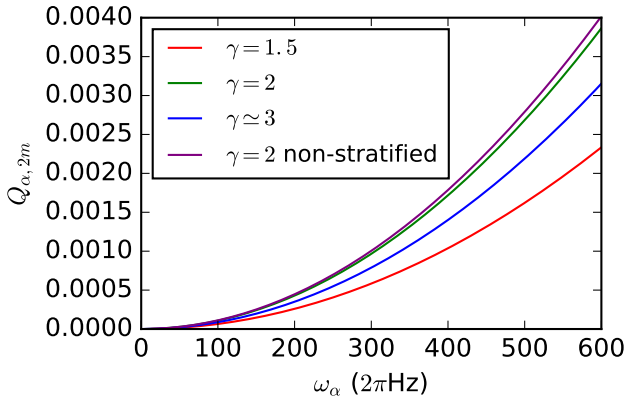

FIG. 1. Tidal coupling coefficient $Q_{\alpha,2m}$ of the $j = 2, n = 1$ g-mode as a function of mode frequency ω_α for different density and stratification models. In this figure we consider a $M = 1.4M_\odot, R = 10$ km NS. The "$\gamma = 2$ non-stratified" curve corresponds to the model with a non-stratified envelope (see Section IV.A.3).

Comparing the results for the three different density models, we see that the scaled frequency and tidal coupling coefficient are both smaller for larger γ. However, a lower mode frequency implies tidal resonance at a larger binary separation, leading to a larger phase shift (for the same $Q_{\alpha,2m}$); see Eq. (12). Figure 1 shows the dependence of $Q_{\alpha,2m}$ on the mode frequency ω_α for different NS density models. We see that for the three models studied here ($\gamma = 1.5, \gamma = 2$ and $\gamma \simeq 3$), the $\gamma = 2$ model yields the largest tidal coupling for given ω_α.

3. *Effect of Non-Stratified Stellar Envelope*

Realistic NSs do not have a constant $\Gamma - \gamma$ throughout the star. To see how non-constant stratification affects the g-modes, here we consider a model where the NS envelope has a zero Brunt Väisälä frequency ($\Gamma - \gamma = 0$). Specifically, we consider a $\gamma = 2$ polytrope with stratification given by

$$\Gamma(r) - \gamma = (\Gamma_0 - \gamma)\left\{\frac{1}{2}\tanh[20(0.8 - r/R)] + \frac{1}{2}\right\}, \quad (30)$$

where Γ_0 is a constant. This gives $\Gamma \simeq \Gamma_0$ for the inner 80% of star and $\Gamma \simeq \gamma$ for the outer 20%. The scaled frequency and tidal coupling coefficient for g-modes in this NS model are given in Table II, where $\bar{\omega}_\alpha$ and $\bar{Q}_{\alpha,2m}$ are defined by (25) - (26) except we now use $\Gamma_0 - \gamma$ instead of $\Gamma - \gamma$.

TABLE II. Scaled frequency and tidal coupling coefficient for $j = 2$ pure g-modes in a $\gamma = 2$ polytropic NS with a non-stratified envelope.[a]

	$\bar{\omega}_\alpha$ $(2\pi\text{Hz})$	$\bar{Q}_{\alpha,2m}$
$n = 1$	± 120.7	1.62×10^{-4}
$n = 2$	± 77.8	3.3×10^{-5}
$n = 3$	± 57.1	1.0×10^{-5}

[a] Note that $\Gamma - \gamma$ is no longer constant in this model, and the definitions of $\bar{\omega}_\alpha$ and $\bar{Q}_{\alpha,2m}$ are given by Eqs. (25)-(26), with Γ replaced by Γ_0 (see Eq. 30).

Comparing Table II with Table I, we see that this non-stratified region tends to decrease the scaled frequency and tidal coupling of g-modes. However, as shown in Figure 1, $Q_{\alpha,2m}$ at given ω_α is barely affected by including a non-stratified envelope.

4. *Effect of Cowling Approximation*

Many works studying NS modes apply the Cowling approximation (e.g. [30, 38, 53]), which ignores $\delta\Psi$. We expect that the Cowling approximation do not affect the result significantly when the mode has multiple nodes in $\delta\Psi$. But for the modes we are interested in (i.e. g-modes with small n, and r-modes with small j which we will discuss later), $\delta\Psi$ usually have few or no node. Therefore it is necessary to investigate whether the Cowling approximation is accurate enough in this case. Table III shows the frequency and tidal coupling coefficient for $j = 2$ g-modes in a $\gamma = 2$ polytropic NS, calculated with the Cowling approximation. We see that applying this approximation barely affects the mode frequency,

TABLE III. Scaled frequency and tidal coupling coefficient for $j = 2$ pure g-modes in a $\gamma = 2$ polytropic NS, using the Cowling approximation.

	$\bar{\omega}_\alpha$ (2πHz)	$\bar{Q}_{\alpha,2m}$
$n = 1$	± 181.5	4.8×10^{-4}
$n = 2$	± 124.7	1.27×10^{-4}
$n = 3$	± 95.7	3.9×10^{-5}

but the tidal coupling $Q_{\alpha,2m}$ is overestimated by 40% - 50%. Therefore, Cowling approximation can only provide a crude approximation for the tidal coupling coefficient.

B. Pure Inertial Modes (I-Modes)

We now consider another limiting case, when the NS has no stratification ($\Gamma = \gamma$). In this case all low-frequency modes are inertial modes (i-modes), whose restoring force is the Coriolis force.

Since we assume that Ω_s is small [compared to the characteristic frequency $(GM/R^3)^{1/2}$], the Lagrangian displacement of an i-mode can be expanded in terms of $\hat{\Omega}_s \equiv \Omega_s (R^3/GM)^{1/2}$:

$$\boldsymbol{\xi}_\alpha = \boldsymbol{\xi}_{\alpha,0} + \hat{\Omega}_s \boldsymbol{\xi}_{\alpha,1} + \hat{\Omega}_s^2 \boldsymbol{\xi}_{\alpha,2} + \cdots , \tag{31}$$

and $\boldsymbol{\xi}_{\alpha,i}$ is independent of $\hat{\Omega}_s$. Similar to Eq. (22), we can decompose the velocity perturbation corresponding to $\boldsymbol{\xi}_{\alpha,i}$ into $u_{jm,i}, v_{jm,i}$ and $w_{jm,i}$. For each i, $u_{jm,i}, v_{jm,i}$ and $w_{jm,i}$ can be nonzero only up to some finite j [35].

Following Ref. [35], we label each i-mode by m and the $j = j_0$ value, the latter given by the largest number such that at least one of $u_{jm,0}, v_{jm,0}$ and $w_{jm,0}$ is nonzero (this j_0 value is the same as l_0 in [35]). In general, there are $(j_0 - m + 1)$ modes for each pair of j_0 and m. The value j_0 is also related to the parity of the mode. Even j_0 corresponds to odd parity modes and odd j_0 even parity modes[1]. Since only the even parity modes couple to the tidal potential, we will only consider modes with odd j_0 (which will be simply labeled j in the discussion below).

1. Inertial Mode Scaling Relations

Table IV shows the frequency and scaled coupling coefficient for $j = 1$ and 3 pure inertial modes for the $\gamma = 1.5$, 2 and $\gamma \simeq 3$ density models. Our results show that to lowest order of $\hat{\Omega}_s$, the mode frequencies $\omega_\alpha, \sigma_\alpha \propto \Omega_s$ and

$$Q_{\alpha,2m} \propto \hat{\Omega}_s^2, \tag{32}$$

therefore we define the scaled tidal coupling coefficient by

$$\hat{Q}_{\alpha,2m} = Q_{\alpha,2m} \hat{\Omega}_s^{-2}. \tag{33}$$

Note that $\hat{Q}_{\alpha,2m}$ is also independent of M and R. The mode frequencies agree with the result from [35] very well, and the scalings agree with the result of [39].

Form Table IV we can see that $Q_{\alpha,2m}$ is mainly determined by j, and decreases as j increases; the $j = 3$ modes have $Q_{\alpha,2m}$ about an order of magnitude smaller than the $j = 1$ mode. Moreover, the $j \geq 5$ modes have $Q_{\alpha,2m}$ about one order of magnitude smaller than the $j \leq 3$ modes. Therefore, the most important contribution to the GW phase shift comes from $j \leq 3$ i-modes.

The $j = m$ i-modes are often referred to as Rossby modes or r-modes; we will call them r-modes from now on to distinguish them from other i-modes. The $j = m = 1$ r-mode is of particular interest. It has $\omega_\alpha/\Omega_s = -1$ and $\sigma_\alpha/\Omega_s = 0$ to the lowest order of Ω_s, and this result is independent of the NS density profile. Our numerical calculation shows that this mode has

$$\sigma_\alpha \propto \hat{\Omega}_s^2 \Omega_s, \tag{34}$$

and the proportionality constant can be found in Table IV. This coefficient should also be affected by the centrifugal distortion of the NS due to rotation, which we do not include in our calculation for Table IV. Kokkotas & Stergioulas [53] gave an analytical calculation of the frequencies of r-modes for an uniform density star with the effect of centrifugal distortion included (but they used Cowling approximation); they found that for this $j = m = 1$ r-mode

$$\sigma_\alpha = -\frac{3}{4} \hat{\Omega}_s^2 \Omega_s. \tag{35}$$

The scaling of this result is the same as ours, but the coefficient is very different. Importantly, our calculation shows that this mode is prograde in the inertial frame ($\sigma_\alpha > 0$ for all our NS models) while theirs retrograde ($\sigma_\alpha < 0$). This suggests that including centrifugal distortion may nontrivially affect the result. We will discuss the effect of distortion by re-calculating this mode in the following subsection.

It is worth noting that the quantity ϵ_α [see (11)], is always $\epsilon_\alpha \simeq \omega_\alpha/2$ for all inertial modes in Table IV. This is because for pure inertial modes in polytropic, non-stratified NS at small $\Omega_{\rm orb}$, $\delta\Psi$ is small and $\langle \mathbf{v}, -\nabla\delta p + \delta\rho \mathbf{g}_0 \rangle \simeq 0$.[2] As a result, integrating equation (14) gives $\langle \mathbf{v}, \mathbf{v} \rangle \simeq \langle \mathbf{v}, i\boldsymbol{\Omega}_\mathbf{s} \times \mathbf{v} \rangle$ and $\epsilon_\alpha \simeq \omega_\alpha/2$.

[1] Here even (odd) parity means that the scalar perturbations of the mode, such as the density perturbation, is conserved (changes sign) upon a parity transformation.

[2] We do not have a good analytical explanation for why $\langle \mathbf{v}, -\nabla\delta p + \delta\rho\mathbf{g}_0 \rangle \simeq 0$. Note that this holds only when $|\omega|, \Omega_s \ll 1$.

TABLE IV. Scaled frequency and tidal coupling coefficient for $j = 1$ and 3 pure i-modes in NSs with different density models.[a]

	$\gamma = 1.5$			$\gamma = 2$			$\gamma \simeq 3$[b]		
	ω_α/Ω_s	σ_α/Ω_s	$\hat{Q}_{\alpha,2m}$[c]	ω_α/Ω_s	σ_α/Ω_s	$\hat{Q}_{\alpha,2m}$	ω_α/Ω_s	σ_α/Ω_s	$\hat{Q}_{\alpha,2m}$
$j=1, m=1$	-1.000	$0.32\hat{\Omega}_s^2$	0.137	-1.000	$0.66\hat{\Omega}_s^2$	0.370	-1.000	$0.90\hat{\Omega}_s^2$	0.559
$j=3, m=2$	0.827	2.827	0.031	0.556	2.556	0.015	0.405	2.405	0.005
	-1.034	0.966	0.010	-1.100	0.900	0.010	-1.151	0.849	0.005
$j=3, m=1$	1.184	2.184	0.026	1.032	2.032	0.017	0.938	1.938	0.007
	-0.746	0.254	0.014	-0.690	0.310	0.009	-0.656	0.344	0.004
	-1.545	-0.545	0.020	-1.613	-0.613	0.014	-1.655	-0.655	0.006

[a] This calculation ignores centrifugal distortion (but includes the gravitational perturbation), which is a good approximation for all modes except for the $j = m = 1$ mode. See Section IV.B.1-2 for discussion.
[b] Same as the $\gamma \simeq 3$ model used in Table I.
[c] $\hat{Q}_{\alpha,2m} = Q_{\alpha,2m}\hat{\Omega}_s^{-2}$ as defined in Eq. (33).

2. *Effect of Centrifugal Distortion*

For all of our calculations (except for this subsection), we assume that the NS is spherical and ignore distortion due to the finite rotation rate. Here we calculate the modes in a distorted NS to study if including this distortion can nontrivially affect the result. As discussed above, this may be especially important for the $j = m = 1$ r-mode. For the stellar density profile, we assume that the NS is barotropic and obtain the distorted profile iteratively, similar to the method in [54]. The method of calculating modes in a distorted star is summarized in [45].

We find that the correction to ω_α/Ω_s and $\hat{Q}_{\alpha,2m}$ due to distortion are both of order $\hat{\Omega}_s^2$. As a result, this correction is unimportant in most cases. The only exception is the $j = m = 1$ r-mode, where σ_α/Ω_s is also of order $\hat{\Omega}_s^2$. Figure 2 shows the inertial-frame frequency σ_α for two different density models when different approximations are used. We see that when we ignore distortion, we get $\sigma_\alpha > 0$ and $\sigma_\alpha \propto \hat{\Omega}_s^2\Omega_s$. When distortion is included, however, σ_α becomes very close to 0: Our results show that $|\sigma_\alpha|/\Omega_s \lesssim 5 \times 10^{-5}$, which is comparable to the estimated numerical error due to the finite grid size of our calculation. This suggests that this $j = m = 1$ r-mode likely has $\sigma_\alpha/\Omega_s = 0$ or $\mathcal{O}(\hat{\Omega}_s^4)$. Moreover, this result is independent of the density profile used: In Figure 2 we use two different density profiles ($\gamma = 2$ and $\gamma \simeq 3$), and σ_α is clsoe to zero for both models.

3. *Effect of Cowling Approximation*

Kokkotas & Stergioulas [53] calculated the inertial-frame frequencies σ_α of $j = m$ r-modes in a rotationally distorted, incompressible (uniform density) star under Cowling approximation (i.e. ignore $\delta\Psi$). To compare with their result, we also calculate σ_α using Cowling approximation in a distorted $\gamma = 2$ or $\gamma \simeq 3$ NS model (see Fig. 2). We see that under Cowling approximation, the $j = m = 1$ r-mode has $\sigma_\alpha/\Omega_s \propto \hat{\Omega}_s^2$ and the mode is retrograde ($\sigma_\alpha < 0$), which has the same sign as the result (for incompressible stars) in [53]. For our NS models with $\gamma = 1.5$, 2 and $\gamma \simeq 3$, this mode has $\sigma_\alpha/(\hat{\Omega}_s^2\Omega_s) = -0.11, -0.30$ and -0.46 respectively, whereas for $\gamma = \infty$, the analytic (Cowling approximation) result is $\sigma_\alpha/(\hat{\Omega}_s^2\Omega_s) = -0.75$.

Similar to the case for g-modes, Cowling approximation barely affect the result of ω_α and σ_α up to $\mathcal{O}(\Omega_s)$, but produces a nontrivial error in $Q_{\alpha,2m}$ (relative error $\gtrsim 30\%$ for most modes in Table IV). Therefore, Cowling approximation should not be used if we need to obtain a relatively accurate result for tidal coupling and GW phase shift.

4. *Discussion on the $j = m = 1$ R-Mode*

As noted above (see Fig. 2), in our "exact" calculation, which takes account of the rotational distortion and gravitational potential perturbation, the $j = m = 1$ r-mode has zero frequency in the inertial frame. Calculations that neglect either of these effects would give an incorrect result ($\sigma_\alpha/\Omega_s \sim \hat{\Omega}_s^2$). This is important because such incorrect result would imply that for a rapidly rotating NS the mode frequency would lie in the LIGO sensitivity band and the resonance could be detectable due to the large GW phase shift it inflicts [39].

It is useful to understand why this $j = m = 1$ mode has zero frequency. In the $\Omega_s \to 0$ limit, the velocity perturbation associated with this mode is (see Eq. 22)

$$\delta\mathbf{v} \propto r\left(\frac{1}{\sin\theta}\frac{\partial Y_{11}}{\partial\phi}\mathbf{e}_\theta - \frac{\partial Y_{11}}{\partial\theta}\mathbf{e}_\phi\right). \tag{36}$$

This corresponds to a "spin-over" perturbation, i.e., the equilibrium rotation around a different axis. With a finite rotation rate ($\Omega_s \neq 0$), there also exists such a "spin-over" mode. When all the effects (distortion and $\Delta\Psi$) are included, the perturbed state should have the same energy as the unperturbed state, and thus the mode should have zero inertial-frame frequency.

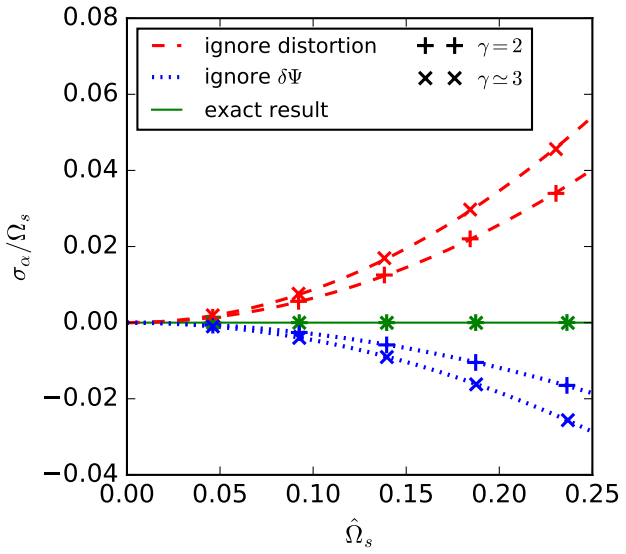

FIG. 2. The inertial-frame frequency σ_α (in units of the spin frequency Ω_s) for the $j = m = 1$ r-mode calculated using different approximations. Crosses and saltires mark the $\gamma = 2$ and $\gamma \simeq 3$ density models, respectively. The red dashed curves correspond to results for a spherical star (i.e. the rotational distortion is ignored) and blue dotted curves correspond to results with Cowling approximation (i.e. $\delta\Psi$ is ignored). The curves are best-fitting results assuming $\sigma_\alpha/\Omega_s \propto \hat{\Omega}_s^2$; we see that this fits the numerical data points well. The green lines show the "exact" results where both $\delta\Psi$ and distortion are included: These results have $\sigma_\alpha/\Omega_s \simeq 0$; the deviation from zero is comparable to the numerical error ($|\sigma_\alpha|/\Omega_s \lesssim 5\times10^{-5}$ for $\hat{\Omega}_s \lesssim 0.25$, **which for a canonical** $1.4M_\odot, 10$**km NS corresponds to spin frequency** $\lesssim 500$**Hz**), so it is likely that this mode has exactly zero inertial-frame frequency or σ_α/Ω_s is of order $\hat{\Omega}_s^4$ or higher.

C. Mixed Modes (Inertial-Gravity Modes)

We now consider modes in rotating, stratified NSs. In such stars, low-frequency modes involve mixing between g-modes and i-modes. Most of these mixed modes become similar to i-modes when stratification is weak or Ω_s is large, and similar to g-modes when stratification is strong or Ω_s is small. Figure 3 shows our numerical results for ω_α, σ_α and $Q_{\alpha,21}$ for the $m = 1$ mixed modes with strongest tidal coupling. As in Section III, we use the scaled rotation rate, mode frequencies and tidal coupling coefficient given by

$$\frac{\bar{\omega}_\alpha}{\omega_\alpha} = \frac{\bar{\sigma}_\alpha}{\sigma_\alpha} = \frac{\bar{\Omega}_s}{\Omega_s} = \left(\frac{\Gamma-\gamma}{0.01}\right)^{-1/2} M_{1.4}^{-1/2} R_{10}^{3/2}, \quad (37)$$

$$\frac{\bar{Q}_{\alpha,2m}}{Q_{\alpha,2m}} = \left(\frac{\Gamma-\gamma}{0.01}\right)^{-1}. \quad (38)$$

The scaled quantities are independent of $\Gamma-\gamma$, M and R to the lowest order. This allows our results to be easily

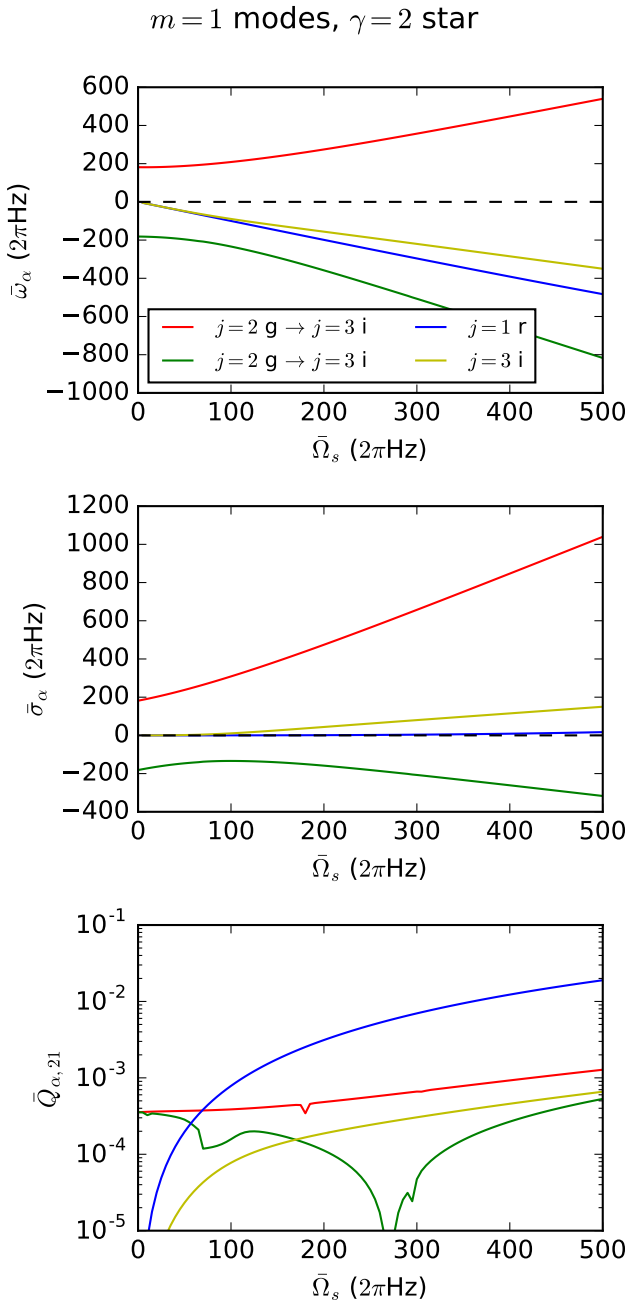

FIG. 3. Scaled rotating (inertial) frame frequency $\bar{\omega}_s$ ($\bar{\sigma}_s$) and tidal coupling coefficient $\bar{Q}_{\alpha,21}$ for the $m = 1$ mixed modes in a rotating and stratified $\gamma = 2$ polytropic NS. The results in this figure are exact for $\Gamma - \gamma = 0.01$, and are accurate to the lowest order [$\hat{\Omega}_s$ and $(\Gamma-\gamma)^{1/2}$ order for frequencies, and $\hat{\Omega}_s^2$ and $(\Gamma-\gamma)$ order for $Q_{\alpha,21}$] otherwise. The mode is labeled by the pure g-mode and pure i-mode they are similar to in the small Ω_s and large Ω_s limits; e.g. "$j = 2$ g $\to j = 3$ i" denotes a mode that is similar to a $j = 2$ g-mode when $\Omega_s \to 0$ and is similar to a $j = 3$ i-mode when Ω_s is large. Modes that have zero frequency at $\Omega_s = 0$ are labeled by the i-mode they are similar to at large Ω_s; e.g. "$j = 3$ i" denotes a mode that becomes similar to a $j = 3$ i-mode at large Ω_s.

adapted for different values of $\Gamma - \gamma$, M and R.

Four modes shown in Figure 3. Two of these are the $j = 2, m = 1, n = 1$ g-modes in the limit $\Omega_s \to 0$. As Ω_s increases, the frequencies, tidal coupling coefficients and perturbation profiles (eigenfunctions) of the modes change characters and become mixed with i-modes. Towards the right side of the plot (high Ω_s), the effect of rotation dominates and these two modes asymptotically become two of the three $j = 3, m = 1$ i-modes discussed in Section B. The other two modes shown in Fig. 3 are another $j = 3, m = 1$ i-mode and the $j = m = 1$ r-mode. As $\Omega_s \to 0$, they both have $\omega_\alpha \to 0$, indicating that they do not become g-modes in this limit.

Figure 4 shows the comparison of σ_α and $Q_{\alpha,21}$ of the $j = m = 1$ r-mode in a stratified NS and an unstratified NS; we see that there is no noticeable difference between the two results, suggesting that this mode is unaffected by stratification. Since we already know (see Section IV.B) that this mode has an inertial-frame frequency that satisfies $|\sigma_\alpha| \ll \hat{\Omega}_s^2 \Omega_s$ when there is no stratification, we conclude that the same inequality applies for realistic stratified NSs.

The $j = 3,\ m = 1$ i-mode is affected by stratification in an interesting way. Figure 5 shows the comparison of σ_α and $Q_{\alpha,21}$ of this $j = 3, m = 1$ i-mode in a stratified NS and an unstratified NS. We see that stratification causes σ_α to decrease and $Q_{\alpha,21}$ to increase. The effect of stratification is most significant when $\Omega_s \to 0$: the decreased σ_α and increased $Q_{\alpha,21}$ makes the GW phase shift converge to a finite value as $\Omega_s \to 0$, while when there is no stratification the GW phase shift goes to zero at $\Omega_s \to 0$. We will discuss the GW phase shift of this mode in more detail in Section V.

Figure 6 is similar to Fig. 3 but shows the $m = 2$ mixed modes. It shows two modes which are the two $j = 2,\ m = 2,\ n = 1$ g-modes for $\Omega_s \to 0$. Similar to the $m = 1$ g-modes, their frequencies and perturbation profiles change as Ω_s increases, and for large Ω_s they asymptotically become the two $j = 3,\ m = 2$ i-modes. Note that the retrograde g-mode becomes a prograde i-mode as Ω_s increases (the purple lines in the figure), therefore the inertial frame frequency σ_α crosses zero at some intermediate Ω_s (for our NS model this happens at $\bar{\Omega}_s \simeq 110 \cdot 2\pi\text{Hz}$). When σ_α is small, the GW phase shift can be significantly boosted as we see from Eq. (12) that $\Delta\Phi \propto \sigma_\alpha^{-1}$.

A major goal of this paper is to study whether tidal coupling can be increased by the mixing between g-modes and i-modes in the regime when the effects of stratification and rotation are comparable. In this regime the perturbation profiles of the modes can be significantly different from pure g-modes or pure i-modes, which in principle may allow the corresponding $Q_{\alpha,2m}$ to increase. However, Figures 3 and 6 show that the tidal coupling coefficient does not significantly increase in this regime; instead, for some modes the tidal coupling is suppressed (e.g. the green curve in Figure 3 and the blue curve in Figure 6). Therefore, the mixing between g-modes and i-modes in general does not increase the GW phase shift by increasing the tidal coupling coefficient, but mainly by changing the inertial-frame mode frequency.

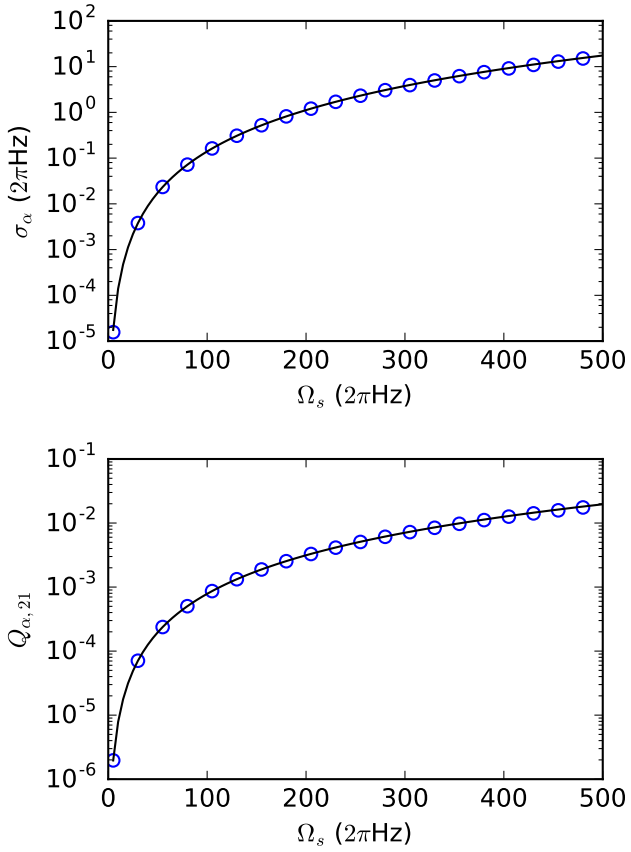

FIG. 4. Inertial-frame frequency σ_α and tidal coupling coefficient $Q_{\alpha,21}$ of the $j = m = 1$ r-mode in a $\gamma = 2$ polytropic NS with $M = 1.4 M_\odot$ and $R = 10$km. Blue circles are the results for a stratified NS with $\Gamma - \gamma = 0.01$ (corresponding to the blue curve in Figure 3), and black curves are the results for an unstratified NS. We see that the two results are identical, even at $\Omega_s \to 0$ where the effect of stratification is much stronger than that of rotation. Note that the results shown in this figure (and in other figures of Section IV.C) do not include the effect of the rotational distortion; when the effect is included, σ_α for the $j = m = 1$ r-mode is zero to the accuracy of our calculation.

We note that as a result of mode mixing, there are some ambiguities in tracing the evolution of different modes as Ω_s varies. In fact, in Figure 3 and Figure 6 some of the curves do not strictly follow a single mode. As the example depicted in Fig. 7 shows, two adjacent modes may exchange their perturbation profiles and the tidal coupling coefficients due to mixing. When this happens, we cross into the other mode which preserves the perturbation profile we are interested in and has a larger tidal coupling. This is the reason for the few small dips in bottom panels of Figs. 3 and 6.

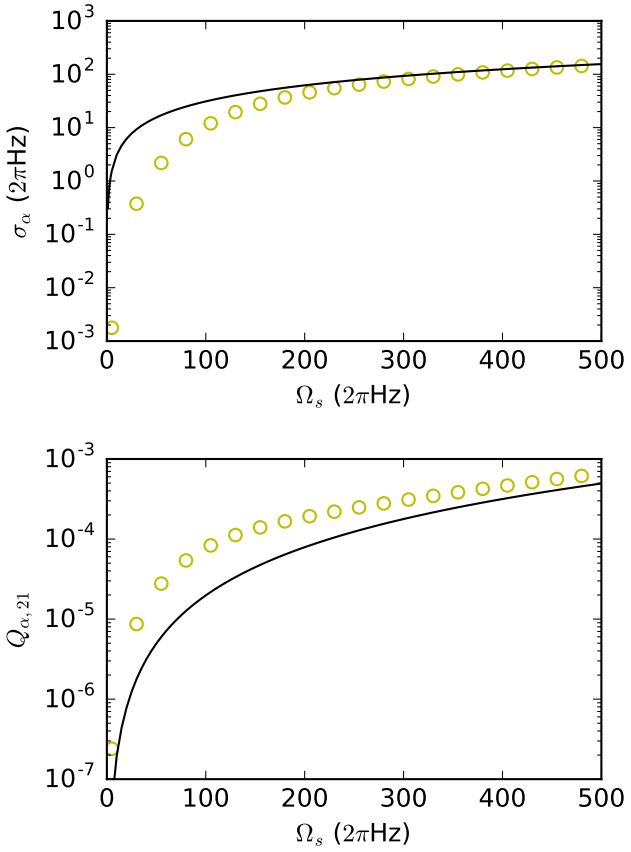

FIG. 5. Inertial-frame frequency σ_α and tidal coupling coefficient $Q_{\alpha,21}$ of the $j=3, m=1$ i-mode that does not become a g-mode in a stratified NS when $\Omega_s = 0$ (the yellow curve in Fig. 3) in a $\gamma = 2$ polytropic NS with $M = 1.4M_\odot$ and $R = 10$km. The yellow circles are the results for a stratified NS with $\Gamma - \gamma = 0.01$ (corresponding to the yellow curve in Fig. 3), and the black curves are results for an unstratified NS. We see that σ_α is significantly decreased for small Ω_s and the tidal coupling coefficient is increased due to the stratification.

V. GW PHASE SHIFT DUE TO TIDAL RESONANCE

Given the frequency and tidal coupling coefficient of the NS oscillation modes, we can calculate the GW phase shift $\Delta\Phi$ due to each tidal resonance. In this section we first consider $\Delta\Phi$ due to pure (non-rotating) g-mode resonance in different NS models. Then we discuss $\Delta\Phi$ for mixed modes, emphasizing two cases where the mixing between g-modes and i-modes affects the GW phase shift in a nontrivial way.

A. Pure g-Modes

We begin by considering the $\Omega_s = 0$ case, and all low-frequency modes are pure g-modes. From Eqs. (12), (25)

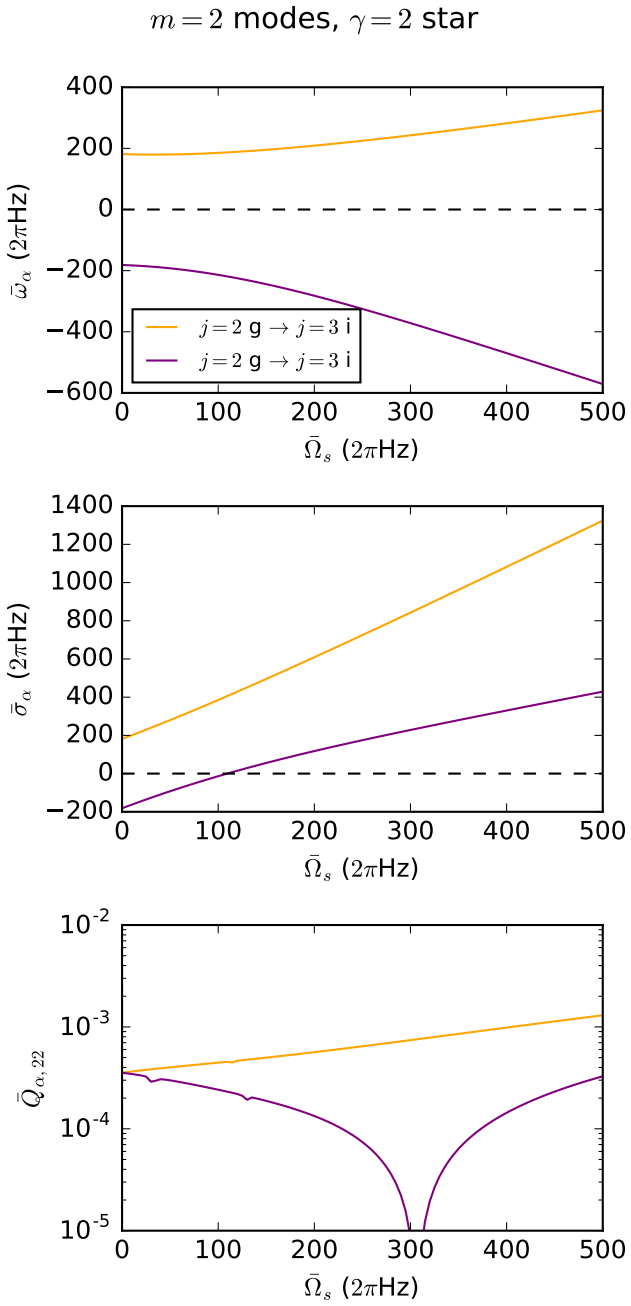

FIG. 6. Same as Figure 3 but for the $m = 2$ modes.

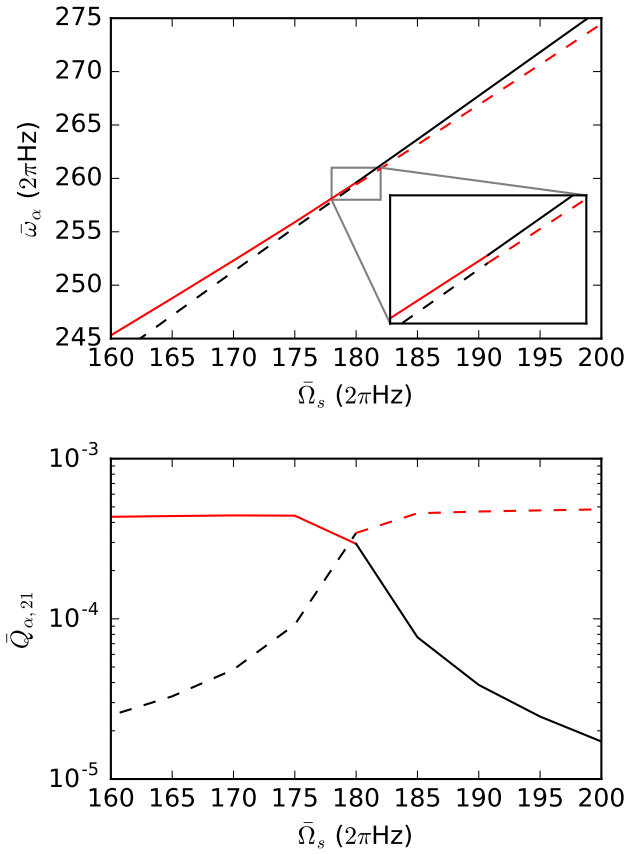

FIG. 7. "Crossing" of two adjacent modes. The solid and dashed curves mark two adjacent modes. We see that as they become close to each other at $\simeq 180 \cdot 2\pi$Hz, they avoid crossing each other but exchanges perturbation profiles. The exchange is apparent if we look at $\bar{Q}_{\alpha,21}$ of the two modes. In order to trace the mode we are most interested in (i.e., the mode with larger tidal coupling), we choose to consider the red colored branches as a single mode. The mode shown here is the $j = 2,\ m = 1$ modified g-mode with positive frequency shown in Fig. 3 (the red curve).

and (26), we find that for aligned spin ($\Theta = 0$),

$$\begin{aligned}\Delta\Phi &= -0.060 \left(\frac{R_{10}}{M_{1.4}}\right)^5 \frac{2}{q(1+q)} \left(\frac{\Gamma-\gamma}{0.01}\right) \\ &\quad \times \left(\frac{\bar{f}_\alpha}{100\,\mathrm{Hz}}\right)^{-2} \left(\frac{\bar{Q}_{\alpha,22}}{10^{-3}}\right)^2 \\ &= -0.060 \left(\frac{R_{10}^8}{M_{1.4}^6}\right) \frac{2}{q(1+q)} \left(\frac{f_\alpha}{100\,\mathrm{Hz}}\right)^2 \\ &\quad \times \left(\frac{\bar{f}_\alpha}{100\,\mathrm{Hz}}\right)^{-4} \left(\frac{\bar{Q}_{\alpha,22}}{10^{-3}}\right)^2, \end{aligned} \tag{39}$$

where $f_\alpha = \omega_\alpha/(2\pi)$ is the mode frequency, and $\bar{f}_\alpha = \bar{\omega}_\alpha/(2\pi)$ and $\bar{Q}_{\alpha,22}$ can be directly read off from Tables I-III for different NS models. Figure 8 shows the magnitude of the phase shift $\Delta\Phi$ due to tidal resonance with

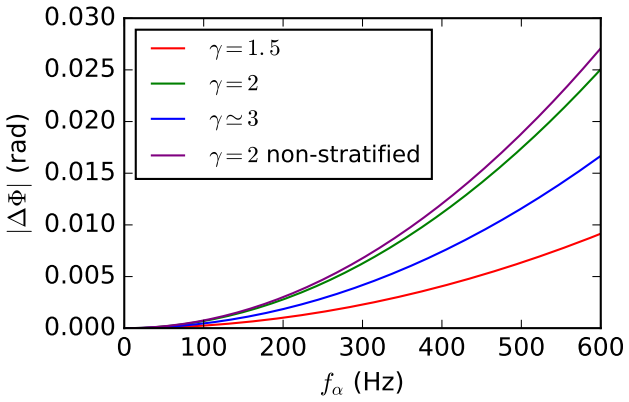

FIG. 8. GW phase shift $|\Delta\Phi|$ due to tidal resonance with the $j = 2, n = 1$ g-mode as a function of mode frequency $f_\alpha = \omega_\alpha/2\pi$ (also the GW frequency) for different NS density and stratification models. The sign of $\Delta\Phi$ is negative. In this figure we consider a $M = 1.4M_\odot$, $R = 10$km NS in an equal-mass binary with aligned spin ($\Theta = 0$). The "$\gamma = 2$ non-stratified" curve corresponds to the model with a non-stratified envelope (see Section IV.A.3).

the $j = 2, m = 2, n = 1$ g-mode in a canonical NS binary ($M = 1.4M_\odot$, $R = 10$ km and $q = 1$) with different density and stratification profiles, as a function of the mode frequency f_α (which is also the inertial frame frequency, and is equal to the GW frequency). We see that among the three density models we considered, $\gamma = 2$ gives the largest GW phase shift for given f_α. Meanwhile, including a non-stratified envelope barely affects the relation between the GW phase shift and f_α. For f_α at ~ 300 Hz, we find $|\Delta\Phi| \lesssim 0.01$ for the canonical NS binaries.

It is important to recognize the strong dependence of Eq. (39) on the mass and radius of the NS. For example, if we consider a $M = 1.2M_\odot$, $R = 13$ km NS (which is entirely allowed or even preferred by empirically constrained nuclear equations of state; see [55]; also note that the measured NS mass ranges from $1.17M_\odot$ to $2M_\odot$), the phase shift in Fig.8 should be increases by a factor ($\propto R^8/M^6$) of 20.6 !

B. Pure Inertial Modes

With finite NS rotation (but no stratification), we have $\sigma_\alpha \propto \Omega_s$ and $Q_{\alpha,2,m} \propto \Omega_s^2$. Equation (12) can be written as

$$\begin{aligned}\Delta\Phi &= \mp 0.0027 \left(\frac{R_{10}^8}{M_{1.4}^6}\right) \frac{2}{q(1+q)} \left(\frac{\epsilon_\alpha |\sigma_\alpha|}{\Omega_s^2}\right)^{-1} \\ &\quad \times \left(\frac{Q_{\alpha,2m}}{0.02\hat{\Omega}_s^2}\right)^2 \left(\frac{f_s}{500\,\mathrm{Hz}}\right)^2 \left|\mathcal{D}^{(2)}_{m\pm 2}\right|^2, \end{aligned} \tag{40}$$

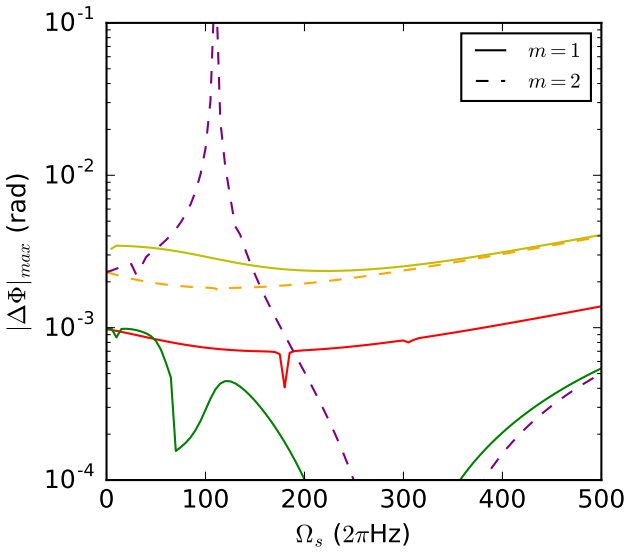

FIG. 9. Maximum GW phase shift $|\Delta\Phi|_{\rm max}$ (i.e. assuming a spin-orbit inclination which gives the largest $|\Delta\Phi|$) as a function of the NS rotation rate Ω_s, for different modes in a $\gamma = 2$ polytropic NS with $M_{1.4} = R_{10} = 1$ and $\Gamma - \gamma = 0.01$, with an equal-mass companion. The solid (dashed) lines denote the $m = 1$ ($m = 2$) modes. Each line corresponds to the mode with the same color shown in Fig. 3 (for $m = 1$) or Fig. 6 (for $m = 2$). Note that the $j = m = 1$ r-mode (the blue lines in Fig. 3) is not included here because its inertial-frame frequency is essentially zero.

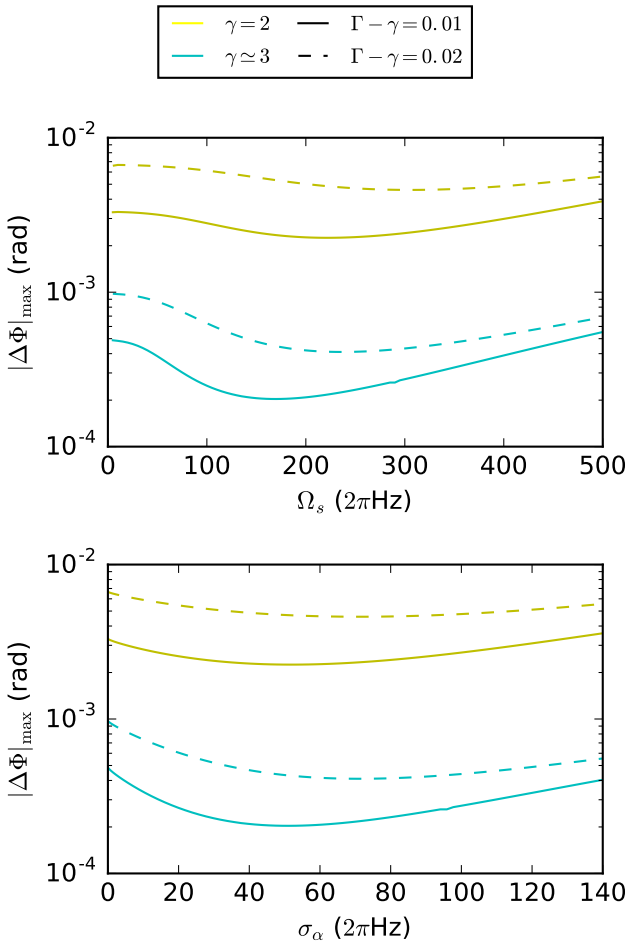

FIG. 10. Maximum GW phase shift $|\Delta\Phi|_{\rm max}$ for one of the $j = 3$, $m = 1$ i-modes (the yellow curves in Fig. 3) for different stellar models. The NS parameters are $M_{1.4} = R_{10} = 1$. Upper panel: $|\Delta\Phi|_{\rm max}$ as a function of stellar spin Ω_s. Lower panel: $|\Delta\Phi|_{\rm max}$ as a function of the inertial-frame frequency (which is equal to the GW frequency). Different color denotes different density models and the solid and dashed lines denote relatively low ($\Gamma - \gamma = 0.01$) and high ($\Gamma - \gamma = 0.01$) stratification, respectively.

where $f_s = \Omega_s/(2\pi)$ is the NS rotation frequency, the upper (lower) sign applies to modes with $\sigma_\alpha > 0$ ($\sigma_\alpha < 0$), which are excited by the $m' = 2$ ($m' = -2$) tidal potential. The relevant Wigner functions are

$$|\mathcal{D}^{(2)}_{22}| = \cos^4\frac{\Theta}{2}, \tag{41}$$

$$|\mathcal{D}^{(2)}_{2-2}| = \sin^4\frac{\Theta}{2}, \tag{42}$$

$$|\mathcal{D}^{(2)}_{12}| = 2\cos^3\frac{\Theta}{2}\sin\frac{\Theta}{2}, \tag{43}$$

$$|\mathcal{D}^{(2)}_{1-2}| = 2\sin^3\frac{\Theta}{2}\cos\frac{\Theta}{2}, \tag{44}$$

where Θ is the spin-orbit misalignment angle. From Table IV we see that $Q_{\alpha,2m} \lesssim 0.02\hat{\Omega}_s^2$, thus pure i-modes give rise to a negligible $\Delta\Phi$ unless the star has $R^8_{10}/M^6_{1.4} \gg 1$.

C. Mixed Modes

In the presence of NS rotation and stratification, we write Eq. (12) (using Eqs. 37 and 38) in the form

$$\begin{aligned}\Delta\Phi &= \mp 0.060\left(\frac{R_{10}}{M_{1.4}}\right)^5\frac{2}{q(1+q)}\left(\frac{\Gamma-\gamma}{0.01}\right)\\ &\times\left(\frac{\bar{f}_\alpha}{100\,\rm Hz}\right)^{-2}\left(\frac{\bar{Q}_{\alpha,2m}}{10^{-3}}\right)^2\left(\frac{2\pi f_\alpha}{\epsilon_\alpha}\right)\left|\mathcal{D}^{(2)}_{m\pm2}\right|^2\\ &= \mp 0.060\left(\frac{R^8_{10}}{M^6_{1.4}}\right)\frac{2}{q(1+q)}\left(\frac{f_\alpha}{100\,\rm Hz}\right)^2\\ &\times\left(\frac{\bar{f}_\alpha}{100\,\rm Hz}\right)^{-4}\left(\frac{\bar{Q}_{\alpha,2m}}{10^{-3}}\right)^2\left(\frac{2\pi f_\alpha}{\epsilon_\alpha}\right)\left|\mathcal{D}^{(2)}_{m\pm2}\right|^2\end{aligned} \tag{45}$$

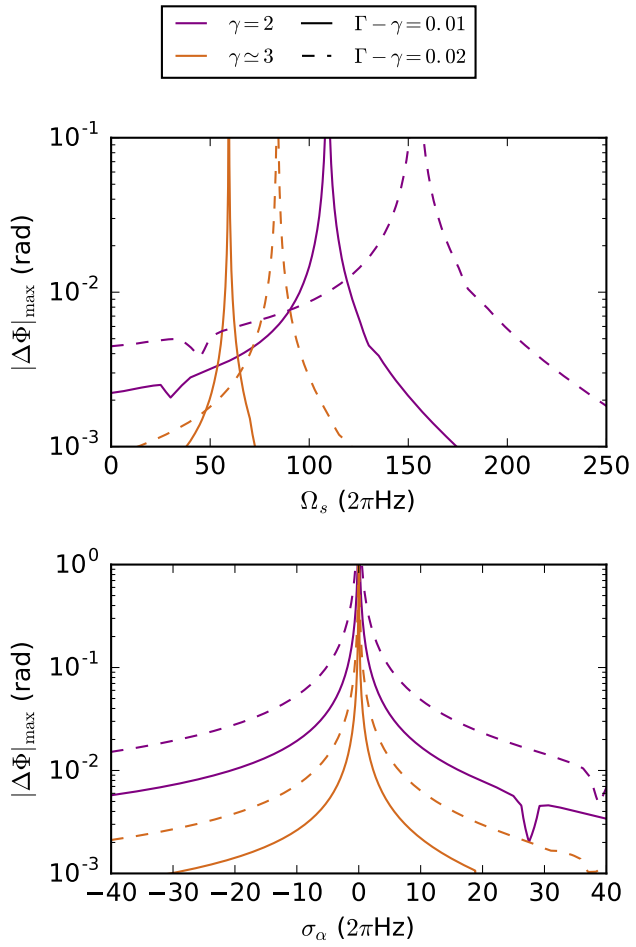

FIG. 11. Similar to Figure 10, but for the modified $m = 2$ g-mode that has σ_α zero crossing in frequency (purple curves in Fig. 6).

where $f_\alpha = |\sigma_\alpha|/(2\pi)$ is the absolute value of the mode frequency, and $\bar{f}_\alpha = |\bar{\sigma}_\alpha|/(2\pi)$ and $\bar{Q}_{\alpha,2m}$ can be read off from Figs. 3-6 for different NS models and modes. In Eq. (45), the upper (lower) sign applies to modes with $\sigma_\alpha > 0$ ($\sigma_\alpha < 0$), i.e., the prograde (retrograde) modes with respect to the spin axis in the inertial frame, which are excited by the $m' = 2$ ($m' = -2$) tidal potential.

Figure 9 shows the GW phase shift at the optimal inclination (i.e., for the value of Θ that maximizes $|\mathcal{D}^{(2)}_{m\pm2}|$) for the modes depicted in Figs. 3 and 6. Note that the phase shift of the $j = m = 1$ r-mode (the blue curves in Fig. 3) is now shown here because its frequency σ_α is essentially zero. We see that for most modes with canonical NS parameters ($M_{1.4} = R_{10} = 1$), the GW phase shift is much less than unity. In fact, with two exceptions (which we will discuss in the next paragraphs), the GW phase shift of a mixed mode is not significantly larger than that of the corresponding pure g-mode when rotation is ignored, or the corresponding pure i-mode when stratification is ignored. This comes about because the tidal coupling $Q_{\alpha,2m}$ is usually not significantly enhanced by mode mixing. As a result, for these modes, knowing the pure g-mode and pure i-mode results is enough to give a good estimate of the GW phase shift.

There are two cases where the combination of rotation and stratification significantly enhances the GW phase shift, and an estimate of $\Delta\Phi$ based on pure i-modes or pure g-modes would prove inadequate. The first case concerns the i-modes that are significantly modified by stratification. An example of this is the yellow mode shown in Fig. 3. When $\Omega_s \to 0$, this mode has $\sigma_\alpha \to 0$ and does not become any of the g-modes; however, the mode frequency and tidal coupling are both significantly affected by stratification (see Fig. 5). As a result, we see in Figure 9 that $\Delta\Phi$ for this mode converges to a finite value as $\Omega_s \to 0$. In particular, for a wide range of Ω_s (including $\Omega_s \to 0$), $\Delta\Phi$ of this mode is larger than all other modes shown in Fig. 9. To study this mode in more details, we plot the maximum GW phase shift as a function of Ω_s and σ_α for different stellar models in Figure 10. We see that $|\Delta\Phi|$ decreases as γ increases; this agrees with the fact that $Q_{\alpha,21}$ decreases when γ increases (see Table IV). Also, $|\Delta\Phi|$ increases when $\Gamma - \gamma$ increases; we find that $|\Delta\Phi| \propto \Gamma - \gamma$ at $\Omega_s \to 0$, which is a scaling relation similar to pure g-modes. For larger Ω_s, stratification affects $\Delta\Phi$ less significantly. Moreover, this mode maintains a relatively large (compared to other modes) and nearly constant (varying by $\lesssim 50\%$) $\Delta\Phi$ as σ_α varies from zero to a few hundred Hz, while most other modes have zero $\Delta\Phi$ at $\sigma_\alpha \to 0$ (because for those modes small σ_α requires either stratification or rotation to be small). Note that this mode has very small frequency ($\sigma_\alpha \ll \Omega_s$) for small Ω_s; therefore it is necessary to consider whether rotational distortion affects the above results. It turns out that rotational distortion only modifies σ_α and $\Delta\Phi$ slightly.

Another important case is when the inertial-frame frequency σ_α becomes small due to the combined effects of stratification and rotation. This occurs when a retrograde mode (with $\omega_\alpha < 0$) gets "dragged" by the NS rotation, so that σ_α increases and changes sign as Ω_s increases. As a result, σ_α becomes zero for a particular value of Ω_s, which causes the GW phase shift $\Delta\Phi$ to diverge (since $\Delta\Phi \propto 1/|\sigma_\alpha|$).[3] An example is the $m = 2$ purple mode depicted in Fig. 6, which has a negative σ_α for $\Omega_s \to 0$ ("retrograde") and positive σ_α ("prograde") for large Ω_s. We see from Fig. 9 that $|\Delta\Phi|_{\max}$ diverges at $\Omega_s \simeq 110 \cdot 2\pi$Hz. Figure 11 shows the maximum GW phase shift due to this $m = 2$ mixed mode as a function of Ω_s and σ_α for different NS models. We see that for larger γ, the zero crossing ($\sigma_\alpha = 0$) happens at smaller Ω_s and the peak is narrower, while for larger $\Gamma - \gamma$, the zero crossing happens at larger Ω_s and the peak is wider. For $\gamma = 2, \Gamma - \gamma = 0.02$ (which gives the

[3] It is in principle possible for $\Delta\Phi$ to diverge due to ϵ_α crossing zero; but this never happens for the modes studied in this paper.

largest $|\Delta\Phi|_{\rm max}$ among the four sets in Fig. 11), we see that $|\Delta\Phi|_{\rm max} \gtrsim 0.01$ rad for a $\sim 100 \cdot 2\pi$Hz range in σ_α (which corresponds to a ~ 50 Hz range in the GW frequency). This relatively large width suggests that there is an appreciable chance for the system to have a combination of spin and stratification profile that gives a small enough $|\sigma_\alpha|$ to cause a significant GW phase shift.

D. Summary: GW Phase Shift for Different GW Frequencies

In order to relate our results to potential future observations, we summarize here the GW phase shifts we expect to see at different GW frequencies. Note that the GW frequency ($f_{\rm GW}$) is equal to the absolute value of the inertial-frame mode frequency (since we only consider the tidal potential with $m' = \pm 2$), i.e. $f_{\rm GW} = f_\alpha = |\sigma_\alpha|/(2\pi)$. For convenience, we consider a NS with $M_{1.4} = R_{10} = 1$ and an equal-mass companion, but results for other NS/binary parameters can be obtained by appropriate scalings.

For $f_{\rm GW} \lesssim 20$ Hz, the most significant GW phase shift comes from the tidal resonance of zero-crossing mixed modes (or modified g-modes); see the purple-lined mode shown in Figs. 6 and 9) with small σ_α. These modes can have large GW phase shift (even $\gtrsim 1$ rad), and the $|\Delta\Phi|$ is larger for smaller σ_α (and thus smaller $f_{\rm GW}$). Note that to have a small σ_α requires the NS to have a right combination of stratification and rotation (see Fig. 11). For a given NS binary, the probability that the parameters of the system gives a small σ_α is relatively low.

Another major source of GW phase shift at low frequency ($f_{\rm GW} \lesssim 100$ Hz) is the stratification-modified i-mode (see the yellow-lined mode in Figs. 3 and 9; see also Fig. 10). For these modes the GW frequency is determined by the spin rate and stratification together, but the phase shift is mainly determined by the strength of stratification. As a result, there is little correlation between phase shift and GW frequency. For typical stratification ($\Gamma - \gamma \sim 0.01$), the phase shift is $\sim 10^{-3}$ to 10^{-2} rad.

For higher frequency ($f_{\rm GW} \gtrsim 100$ Hz), the most significant GW phase shift can come from g-mode, i-mode or mixed modes, depending on the parameters of the system. These modes share the common features that the GW phase shift tends to increase as $f_{\rm GW}$ increases, while $f_{\rm GW}$ tends to increase when stratification and spin rate increase. NSs with large stratification and/or spin rate will have modes at relatively high frequency (a few hundred Hz) that give a relatively large ($\gtrsim 0.01$ rad) GW phase shift.

VI. SUMMARY

We have presented a comprehensive study on the resonant tidal excitation of neutron star (NS) oscillation modes in coalescing compact binaries. Such "resonant tide" may affect the gravitational waveforms from the binary inspiral, and could potentially provide a clean window for studying NSs using gravitational waves. Our study goes beyond previous works in that we treat the effects of NS rotation and stratification exactly (using a newly developed spectral code for NS oscillations) – this exact calculation reveals several features of the resonant tide that are not present in previous works. The main results of our paper are summarized as follows.

- Given the various uncertainties associated with the NS equation of state and in preparation for future studies of NSs using GWs, we have adopted parameterized polytropic models that characterize the density and stratification profiles of the NS. Such a parameterization provides a "survey" for various possible NS models. Throughout the paper, we have presented scaling relations for the NS oscillation mode frequency, tidal coupling coefficient and the GW phase shift associated with a resonance. Thus, while our numerical results and figures are often specific to a particular NS model, they can be rescaled when a different NS model is considered.

- We have developed a new spectral code to calculate the oscillation modes of rotating NSs, with an exact treatment of the Coriolis force. This exact (non-perturbative) treatment allows us to obtain the mapping of various modes as a function of the rotation rate (see Figs. 3-4). Our spectral code can also include the effects of rotational distortion of the unperturbed star and the gravitational perturbation (i.e., without using the Cowling approximation). We find that although adopting the Cowling approximation barely affects the mode frequency, it can cause appreciable overestimate of the tidal coupling coefficient and the GW phase shift. Overall, while these high-order effects (rotational distortion and gravitational perturbation) do not qualitatively change the tidal excitation property of most oscillation modes, there is one important exception: We have shown that when all these effects are included, the $j = m = 1$ r-mode has essentially zero frequency, whereas approximate calculations would give $\sigma_\alpha/\Omega_s \sim \hat{\Omega}_s^2$. (see Section IV.B.4 for more details). This is important because it implies that the $j = m = 1$ r-mode cannot be tidally excited during binary inspiral.

- For pure g-modes (with negligible rotation), the mode frequency f_α (which is also the corresponding GW frequency at resonance) depends on the stratification, and the GW phase shift $|\Delta\Phi|$ is always

$\lesssim 0.01$ for canonical NSs ($M = 1.4M_\odot$, $R = 10$ km) and equal-mass binaries (Fig. 8). However, $\Delta\Phi$ increases as R^8/M^6 (Eq. 38) and can become significant for low-mass NSs with larger radii. For pure inertial modes (with no stratification), the phase shift is typically smaller, but it also increases with increasing R^8/M^6 (Eq. 39).

- In the presence of both rotation and stratification, a NS has a spectrum of mixed (inertial-gravity) modes (Figs. 3-4), two of which may lead to appreciable GW phase shift at low frequency (Fig. 9). The first can be thought of as the rotation-modified $m = 2$ g-mode (the purple lines in Fig. 4 and Fig. 9; see also Fig. 11): this mode is retrograde in the rotating frame of the NS, but attains a small inertial-frame frequency σ_α because of rotation. A significant $\Delta\Phi$ can be produced when the NS has an appropriate rotation to give $f_\alpha = |\sigma_\alpha|/(2\pi) \lesssim 20$ Hz. The second mixed mode of interest is the stratification-modified $m = 1$ i-mode (the yellow lines in Fig. 3 and Fig. 9; see also Fig. 10): This mode has a frequency that approaches zero for $\Omega_s \to 0$, but is nevertheless significantly affected by the stratification; as a result, $\Delta\Phi$ for this mode is mainly determined by the stratification and does not depend sensitively on the GW frequency (Fig. 10). The value of $\Delta\Phi$ for this mode is still small ($\lesssim 10^{-2}$) for canonical NSs, but as for all the modes studied in this paper, $|\Delta\Phi|$ increases with increasing R^8/M^6 (Eq. 44).

ACKNOWLEDGMENTS

This work has been supported in part by NASA grant NNX14AP31G and a Simons Fellowship in theoretical physics (DL). WX acknowledges the supports from the Hunter R. Rawlings III Cornell Presidential Research Scholar Program and a special undergraduate research fellowship from the Hopkins Foundation.

Appendix A: Numerical Methods

Here we sketch our numerical methods used to solve for the oscillation modes in a rotating star with a general density profile. For simplicity, we ignore the centrifugal distortion of the equilibrium star in our discussion here, although this can be included using the method discussed in Ref. [45].

1. Scaling of Equations

When solving for the eigenmodes of the generalized eigenvalue problem (13) - (16), it is convenient to use the normalization

$$R = 4\pi G = \rho_c = 1, \tag{A1}$$

where ρ_c is the central density of the star. We can define a scaled equilibrium density

$$H(r) \equiv [\rho_0(r)]^{1/N}, \tag{A2}$$

where $N = 1/[\gamma(1) - 1]$, and $\gamma(1)$ is the value of γ evaluated at the stellar surface ($r = 1$), with $\gamma = d\ln p_0/d\ln\rho_0$. We also scale the density and pressure perturbation $\delta\rho$ and δp using

$$b \equiv \delta\rho/H^{N-1}, \quad \Pi \equiv \delta p/H^N, \tag{A3}$$

where we have assumed that $N \geq 1$. Such scaling guarantees the regularity of the solution at the stellar surface.

With the scaled variables, equations (13)-(16) can be written as

$$-i\omega b = -N\delta\mathbf{v}\cdot\nabla H - H\nabla\cdot\delta\mathbf{v}, \tag{A4}$$

$$-i\omega H\delta\mathbf{v} = -H(\nabla\Pi + \nabla\Phi) + \nabla H\left(-N\Pi + \frac{N\gamma}{N+1}\frac{b}{\Lambda}\right) - 2H\boldsymbol{\Omega}_\mathbf{s}\times\delta\mathbf{v}, \tag{A5}$$

$$-i\omega\left(\Pi - \frac{\Gamma}{(N+1)\Lambda}b\right) = \left(\frac{\Gamma}{\gamma} - 1\right)\frac{N\gamma}{N+1}\frac{\delta\mathbf{v}\cdot\nabla H}{\Lambda}, \tag{A6}$$

$$0 = \Delta(\delta\Psi) - H^{N-1}b, \tag{A7}$$

where

$$\Lambda \equiv \frac{\rho_0^{1+1/N}}{(N+1)p_0}. \tag{A8}$$

Note that when the star is exactly polytropic, $\frac{N\gamma}{N+1}$ is always 1 and the above equations reduce to equations (22)-(24) in [45] (with $\lambda = -i\omega$).

Equations (A4)-(A7) are still in 2D; to further reduce the problem we remove the azimuthal dependence by expanding Π, b and $\delta\Psi$ in terms of spherical harmonics:

$$\Pi = \sum_{j=m}^{\infty}\Pi_{jm}Y_{jm}, \quad b = \sum_{j=m}^{\infty}b_{jm}Y_{jm}, \quad \delta\Psi = \sum_{j=m}^{\infty}\Psi_{jm}Y_{jm}, \tag{A9}$$

where Π_{jm}, b_{jm} and Ψ_{jm} are functions of r. Similarly, the velocity perturbation $\delta\mathbf{v} = -i\omega\boldsymbol{\xi}$ can be decomposed into spheroidal and toroidal components:

$$\delta\mathbf{v} = \sum_{j=m}^{\infty}\Big[u_{jm}Y_{jm}\mathbf{e}_r + v_{jm}\left(\partial_\theta Y_{jm}\mathbf{e}_\theta + D_\phi Y_{jm}\mathbf{e}_\phi\right) + w_{jm}\left(D_\phi Y_{jm}\mathbf{e}_\theta - \partial_\theta Y_{jm}\mathbf{e}_\phi\right)\Big], \tag{A10}$$

where u_{jm}, v_{jm}, w_{jm} are functions of r, $\mathbf{e}_r, \mathbf{e}_\theta, \mathbf{e}_\phi$ are unit vectors in r, θ, ϕ direction respectively, and $D_\phi \equiv (\sin\theta)^{-1}\partial_\phi$. The terms with u_{jm}, v_{jm} give the spheroidal component of the velocity perturbation and while the terms with w_{jm} the toroidal component. Thus, the mode is fully described by six sets of variables $(u_{jm}, v_{jm}, w_{jm}, \Pi_{jm}, \Psi_{jm}, b_{jm})$ that only depend on r.

2. Solving the Equations

To solve the eigenvalue problem, we transform (A4)-(A7) into equations of different j components of the variables u, v, w, Π, Ψ, b. We multiply Eqs. (A4), (A6) and (A7) by $\{Y_{jm}\}^*$ and integrate over the 4π solid angle; this effectively projects the equations onto different Y_{jm}. For (A5), we project the equation onto $(Y_{jm}\mathbf{e}_r)$, $(\partial_\theta Y_{jm}\mathbf{e}_\theta + D_\phi Y_{jm}\mathbf{e}_\phi)$ and $(D_\phi Y_{jm}\mathbf{e}_\theta - \partial_\theta Y_{jm}\mathbf{e}_\phi)$ respectively (by multiplying the equation by the conjugate of the projection vector and integrate over 4π radians). For details of this projection and the expression of the projected equations [4], see Ref. [45]. Then we choose a cutoff j (call it $j_{\max}$) and keep only components with $j \le j_{\max}$. For the r direction, we choose a Chebychev grid consisting of N_r points from 0 to 1, which allows us to use spectral method to solve for the modes. The problem is now reduced to a generalized eigenvalue problem of matrices. Note that the use of spectral method requires that the stellar profile (density, stratification, etc.) to be relatively smooth.

For implementation of the boundary conditions, see [45].

3. Limitations of the Method

A major limitation of the method is that we must assume $N \ge 1$ when setting the scaled variables. As a result, this method does not work for stellar models with $N < 1$. Moreover, in practice when N is not an integer the accuracy of the algorithm drops significantly, possibly due to the fact that we are using a spectral method which effectively expands the mode into basis polynomials.

Fortunately, there is an easy way to fix this problem. Since we do not require a constant γ throughout the star (unlike [45]), we can always modify γ near the outer boundary so that most of the star has the density profile we desire, and towards the boundary γ goes to a value which gives a positive integer N and thereby ensuring good performance of our algorithm. In this way, we can obtain a reasonably good approximation for any density profile we need. One example is the $\gamma \simeq 3$ model used in the main text (Section IV).

[1] B. P. Abbott, R. Abbott, T. D. Abbott, M. R. Abernathy, F. Acernese, K. Ackley, C. Adams, T. Adams, P. Addesso, R. X. Adhikari, and et al., Physical Review Letters **116**, 241103 (2016), arXiv:1606.04855 [gr-qc].

[2] B. P. Abbott, R. Abbott, T. D. Abbott, M. R. Abernathy, F. Acernese, K. Ackley, C. Adams, T. Adams, P. Addesso, R. X. Adhikari, and et al., Physical Review X **6**, 041015 (2016), arXiv:1606.04856 [gr-qc].

[3] B. P. Abbott, R. Abbott, T. D. Abbott, F. Acernese, K. Ackley, C. Adams, T. Adams, P. Addesso, R. X. Adhikari, V. B. Adya, and et al., Physical Review Letters **118**, 221101 (2017), arXiv:1706.01812 [gr-qc].

[4] C. Cutler, T. A. Apostolatos, L. Bildsten, L. S. Finn, E. E. Flanagan, D. Kennefick, D. M. Markovic, A. Ori, E. Poisson, and G. J. Sussman, Physical Review Letters **70**, 2984 (1993), astro-ph/9208005.

[5] C. Cutler and K. S. Thorne, in *General Relativity and Gravitation*, edited by N. T. Bishop and S. D. Maharaj (2002) pp. 72–111.

[6] L. Bildsten and C. Cutler, ApJ **400**, 175 (1992).

[7] D. Lai and A. G. Wiseman, Phys. Rev. D **54**, 3958 (1996), gr-qc/9609014.

[8] M. Shibata, K. Taniguchi, and K. Uryū, Phys. Rev. D **71**, 084021 (2005), gr-qc/0503119.

[9] A. Bauswein, N. Stergioulas, and H.-T. Janka, Phys. Rev. D **90**, 023002 (2014), arXiv:1403.5301 [astro-ph.SR].

[10] F. Foucart, M. B. Deaton, M. D. Duez, E. O'Connor, C. D. Ott, R. Haas, L. E. Kidder, H. P. Pfeiffer, M. A. Scheel, and B. Szilagyi, Phys. Rev. D **90**, 024026 (2014), arXiv:1405.1121 [astro-ph.HE].

[11] K. Takami, L. Rezzolla, and L. Baiotti, Physical Review Letters **113**, 091104 (2014), arXiv:1403.5672 [gr-qc].

[12] F. Foucart, R. Haas, M. D. Duez, E. O'Connor, C. D. Ott, L. Roberts, L. E. Kidder, J. Lippuner, H. P. Pfeiffer, and M. A. Scheel, Phys. Rev. D **93**, 044019 (2016), arXiv:1510.06398 [astro-ph.HE].

[13] D. Lai, F. A. Rasio, and S. L. Shapiro, ApJ **420**, 811 (1994), astro-ph/9304027.

[14] C. S. Kochanek, ApJ **398**, 234 (1992).

[15] É. É. Flanagan and T. Hinderer, Phys. Rev. D **77**, 021502 (2008), arXiv:0709.1915.

[16] T. Binnington and E. Poisson, Phys. Rev. D **80**, 084018

[4] The projected equations in Ref. [45] are somewhat different from ours since they assume a strictly polytropic star, but the method of obtaining the equations is similar.

(2009), arXiv:0906.1366 [gr-qc].
[17] T. Damour and A. Nagar, Phys. Rev. D **80**, 084035 (2009), arXiv:0906.0096 [gr-qc].
[18] A. J. Penner, N. Andersson, L. Samuelsson, I. Hawke, and D. I. Jones, Phys. Rev. D **84**, 103006 (2011), arXiv:1107.0669 [astro-ph.SR].
[19] V. Ferrari, L. Gualtieri, and A. Maselli, Phys. Rev. D **85**, 044045 (2012), arXiv:1111.6607 [gr-qc].
[20] T. Damour, A. Nagar, and L. Villain, Phys. Rev. D **85**, 123007 (2012), arXiv:1203.4352 [gr-qc].
[21] J. S. Read, L. Baiotti, J. D. E. Creighton, J. L. Friedman, B. Giacomazzo, K. Kyutoku, C. Markakis, L. Rezzolla, M. Shibata, and K. Taniguchi, Phys. Rev. D **88**, 044042 (2013), arXiv:1306.4065 [gr-qc].
[22] T. Hinderer, A. Taracchini, F. Foucart, A. Buonanno, J. Steinhoff, M. Duez, L. E. Kidder, H. P. Pfeiffer, M. A. Scheel, B. Szilagyi, K. Hotokezaka, K. Kyutoku, M. Shibata, and C. W. Carpenter, Physical Review Letters **116**, 181101 (2016), arXiv:1602.00599 [gr-qc].
[23] D. Lai, MNRAS **270**, 611 (1994), astro-ph/9404062.
[24] T. W. Baumgarte, G. B. Cook, M. A. Scheel, S. L. Shapiro, and S. A. Teukolsky, Phys. Rev. D **57**, 7299 (1998), gr-qc/9709026.
[25] K. Uryū, F. Limousin, J. L. Friedman, E. Gourgoulhon, and M. Shibata, Phys. Rev. D **80**, 124004 (2009), arXiv:0908.0579 [gr-qc].
[26] A. Reisenegger and P. Goldreich, ApJ **426**, 688 (1994).
[27] M. Shibata, Progress of Theoretical Physics **91**, 871 (1994).
[28] E. M. Kantor and M. E. Gusakov, MNRAS **442**, L90 (2014), arXiv:1404.6768 [astro-ph.SR].
[29] A. Passamonti, N. Andersson, and W. C. G. Ho, MNRAS **455**, 1489 (2016), arXiv:1504.07470 [astro-ph.SR].
[30] H. Yu and N. N. Weinberg, MNRAS **464**, 2622 (2017), arXiv:1610.00745 [astro-ph.HE].
[31] H. Yu and N. N. Weinberg, MNRAS **470**, 350 (2017), arXiv:1705.04700 [astro-ph.HE].
[32] W. C. G. Ho and D. Lai, MNRAS **308**, 153 (1999), astro-ph/9812116.
[33] É. É. Flanagan and É. Racine, Phys. Rev. D **75**, 044001 (2007), gr-qc/0601029.
[34] J. Papaloizou and J. E. Pringle, MNRAS **195**, 743 (1981).
[35] K. H. Lockitch and J. L. Friedman, ApJ **521**, 764 (1999), gr-qc/9812019.
[36] A. K. Schenk, P. Arras, É. É. Flanagan, S. A. Teukolsky, and I. Wasserman, Phys. Rev. D **65**, 024001 (2002), gr-qc/0101092.
[37] Y. Wu, ApJ **635**, 674 (2005), astro-ph/0407627.
[38] A. Passamonti, B. Haskell, N. Andersson, D. I. Jones, and I. Hawke, MNRAS **394**, 730 (2009), arXiv:0807.3457.
[39] D. Lai and Y. Wu, Phys. Rev. D **74**, 024007 (2006), astro-ph/0604163.
[40] D. Tsang, J. S. Read, T. Hinderer, A. L. Piro, and R. Bondarescu, Physical Review Letters **108**, 011102 (2012), arXiv:1110.0467 [astro-ph.HE].
[41] N. N. Weinberg, P. Arras, and J. Burkart, ApJ **769**, 121 (2013), arXiv:1302.2292 [astro-ph.SR].
[42] T. Venumadhav, A. Zimmerman, and C. M. Hirata, ApJ **781**, 23 (2014), arXiv:1307.2890 [astro-ph.HE].
[43] N. N. Weinberg, ApJ **819**, 109 (2016), arXiv:1509.06975 [astro-ph.SR].
[44] J. Ballot, F. Lignières, D. R. Reese, and M. Rieutord, A&A **518**, A30 (2010), arXiv:1005.0275 [astro-ph.SR].
[45] D. Reese, F. Lignieres, and M. Rieutord, Communications in Asteroseismology **147**, 65 (2006).
[46] P. N. McDermott, H. M. van Horn, and C. J. Hansen, ApJ **325**, 725 (1988).
[47] C. J. Krüger, W. C. G. Ho, and N. Andersson, Phys. Rev. D **92**, 063009 (2015), arXiv:1402.5656 [gr-qc].
[48] D. D. Doneva, E. Gaertig, K. D. Kokkotas, and C. Krüger, Phys. Rev. D **88**, 044052 (2013), arXiv:1305.7197 [astro-ph.SR].
[49] V. Paschalidis and N. Stergioulas, ArXiv e-prints (2016), arXiv:1612.03050 [astro-ph.HE].
[50] A. Reisenegger and P. Goldreich, ApJ **395**, 240 (1992).
[51] L. S. Finn, MNRAS **227**, 265 (1987).
[52] T. E. Strohmayer, ApJ **417**, 273 (1993).
[53] K. D. Kokkotas and N. Stergioulas, A&A **341**, 110 (1999), astro-ph/9805297.
[54] I. Hachisu, ApJS **61**, 479 (1986).
[55] A. W. Steiner, J. M. Lattimer, and E. F. Brown, ApJ **765**, L5 (2013), arXiv:1205.6871 [nucl-th].